Modification of the Anabaseine pyridine nucleus allows achieving binding and functional selectivity for the α3β4 nicotinic acetylcholine receptor subtype

Carlo Matera,[a] Marta Quadri,[a] Miriam Sciaccaluga,[b] Diego Yuri Pomè,[a] Francesca Fasoli,[d,e] Marco De Amici,[a] Sergio Fucile,[b,c] Cecilia Gotti,[d,e] Clelia Dallanoce,[a,*] Giovanni Grazioso[a]

[a]*Dipartimento di Scienze Farmaceutiche, Sezione di Chimica Farmaceutica "Pietro Pratesi", Università degli Studi di Milano, Via L. Mangiagalli 25, 20133 Milano, Italy*

[b]*I.R.C.C.S. Neuromed, Istituto Neurologico Mediterraneo, Via Atinese 18, 86077 Pozzilli (Isernia), Italy*

[c]*Dipartimento di Fisiologia e Farmacologia, Università di Roma La Sapienza, Piazzale A. Moro 5, 00185 Roma, Italy*

[d]*Consiglio Nazionale delle Ricerche (CNR), Istituto di Neuroscienze, Via Vanvitelli 32, 20129 Milano, Italy*

[e]*Dipartimento di Biotecnologie Mediche e Medicina Traslazionale, Università degli Studi di Milano, Via Vanvitelli 32, 20129 Milano, Italy*

[*]Corresponding author. E-mail: clelia.dallanoce@unimi.it
Phone: +39 02 50319327. Fax: +39 02 50319359.

Abstract

We report the design, synthesis and pharmacological screening of a group of analogues of anabaseine **2**, a naturally occurring unselective nicotinic agonist. The novel nAChR ligands **5-15** were planned following a molecular modeling analysis which suggested the replacement of the pyridine ring of **2** with a 3-substituted benzene ring as a means to gain selectivity for the α3β4 nAChR subtype. Overall, from binding experiments, the synthesized compounds showed high values of α3β4 affinity and α3β4 vs α4β2 selectivity, although they poorly discriminated the homomeric α7 subtype. The three analogues **6**, **12** and **13** were also evaluated in electrophysiological assays, and **12** [6-(3-iodophenyl)-2,3,4,5-tetrahydropyridine] emerged as a rather interesting nicotinic ligand. Indeed, in addition to a noteworthy affinity (K_i = 4.7 nM) for the α3β4 subtype and to an excellent α3β4 vs α4β2 subtype selectivity (806-fold), compound **12** selectively activated the α3β4 nAChR (EC_{50} = 7.4 μM) while eliciting a negligible response at the α7 subtype and no effect at the α4β2 subtype.

Keywords: Neuronal nicotinic acetylcholine receptors - Molecular modeling - Design - Anabaseine-related derivatives - α3β4 nicotinic ligands - Binding affinity - Functional activity/selectivity

1. Introduction

Neuronal nicotinic acetylcholine receptors (nAChRs) are a heterogeneous family of ligand-gated cation channels formed by homo- or hetero-pentameric combinations of α and β subunits ubiquitously expressed in the central (CNS) and peripheral (PNS) nervous systems [1-3]. nAChR subtypes share a common basic structure but their pharmacological and functional properties depend on their subunit composition. The α4β2 and α7 nAChR subtypes are widely expressed in the CNS [4,5], while the α3β4 subtype is mainly localized in the PNS [6] and is highly concentrated in a few brain regions, the medial habenula (MHb) and the interpeduncular nucleus (IPN), and in the pineal gland [7,8].

The α4β2 and α7 nAChR subtypes modulate cognition, anxiety, pain and neuroprotection [9-13], and new selective ligands for these two subtypes are frequently reported in the recent literature [14,15]. On the other hand, the nAChRs containing the α3β4* subunits (the asterisk denotes the possible presence of additional subunits) mediate ACh-induced fast excitatory ganglionic transmission and control the autonomic functions [6,16]. Although the α3β4 nAChR is not the predominant subtype in the brain, recent studies have suggested its relevant role in influencing the behavioral effects of nicotine, the nicotine dependence and some manifestations of nicotine withdrawal [17,18]. It has also been shown that injection of α3β4 nAChR antagonists into the MHb decreases self-administration not only of nicotine [19] but also of multiple abused drugs [20].

Recently, a series of linkage analyses indicated that variants in the human α3-α5-β4 nAChR subunit gene cluster on chromosome 15q24-25.1 are involved in the risk of nicotine dependence, smoking and lung cancer [21], and two of the clustered nAChR genes (α3 and β4) are significantly over-expressed in small-cell lung carcinoma (SCLC) cells, an

aggressive form of lung cancer that is closely related to cigarette smoking [22]. The identification of highly potent and selective α3β4 nAChR ligands may thus be very useful not only to treat nicotine dependence, but also in view of their application in the lung cancer therapy.

To date, the crystal structures of the homologue acetylcholine-binding proteins (AChBPs) have contributed to elucidating the molecular determinants of ligand receptor binding [23-25]. AChBP crystal structures in complex with nAChR ligands indicated that agonists may establish water-mediated hydrogen bonds between their hydrogen bond acceptor moieties and residues on the complementary receptor face [26,27]. Experimental evidence by unnatural amino acid mutagenesis has confirmed the existence of these hydrogen bond interactions [28]. Since computational and experimental investigations indicated the presence of several water molecules in the nAChR binding cleft, it has been suggested that a productive interaction between a hydrogen bond acceptor moiety of the ligand and the complementary receptor protein could be mediated by a water molecule [29-31].

In a recent study [31], we computationally analyzed the presence of water molecules as putative hydrogen bond donor/acceptor moieties in the agonist binding site of the α4β2, α3β4 and α7 nicotinic channels. Initially, we evaluated the interactions of the frog toxin epibatidine (−)-**1** (Figure 1), an exceptionally potent albeit nonselective nicotinic agonist, and of its analogue deschloroepibatidine. Then, our theoretical study was applied to derivatives (±)-**3** and (±)-**4** (Chart 1), in which the 3-hydroxyl and 3-hydroxymethyl groups replacing the nitrogen atom of pyridine should surrogate to some extent the role of a water molecule in the ligand-receptor interaction [31]. The presence of the water molecule in the receptor binding cleft was compatible with our experimental data and both (±)-**3** and (±)-**4** retained a good affinity at α3β4 nAChRs coupled with the appearance, for (±)-**3**, of α3β4 vs α4β2 functional

selectivity [31].

In the present study, we applied a parallel approach to anabaseine **2** (Figure 1), one among the pyridine-containing nicotinic alkaloids, which is a toxin that some marine worms use as a chemical defense and as a means for capturing prey. Like epibatidine **1**, anabaseine **2** rather indiscriminately stimulates all nicotinic cholinergic receptors [32], displaying higher potency on neuromuscular ($\alpha1\beta1\gamma\delta$) and neuronal $\alpha7$ receptor nAChRs and evoking lower detectable responses from $\alpha4\beta2$ and $\alpha3\beta4$ subtypes. At the time we started this study, the binding affinity of **2** for $\alpha3\beta4$ nAChRs was unknown [33]. At variance with epibatidine or nicotine, anabaseine is an achiral molecule bearing a tetrahydropyridine ring, whose imine double bond is conjugated with the 3-pyridyl moiety. Thus, the two rings of **2** are almost coplanar, whereas in **1** the six-membered ring is part of the 7-azabicyclo[2.2.1]heptane skeleton and the 2-chloro-5-pyridyl moiety adopts an *exo* orientation. Since we aimed at identifying selective $\alpha3\beta4$ nAChR ligands, in analogy to (±)-**3** and (±)-**4** we initially designed, synthesized and tested derivatives **5** and **6** (Figure 1), in which the 3-pyridyl ring of **2** was replaced by the 3-hydroxybenzene or 3-hydroxymethylbenzene moieties, respectively. Then, we enriched the substitution pattern on positions 3 and 3,5 of the aromatic ring by preparing and testing the group of analogues **7-15** (Figure 1).

Figure 1 to be inserted about here

Herein we report the synthesis and the pharmacological and computational investigations on target compounds **5-15** at neuronal $\alpha3\beta4$, $\alpha4\beta2$ and $\alpha7$ nAChR subtypes. Based on the binding affinity data, we selected derivatives **6**, **12** and **13** to evaluate their functional behavior in electrophysiological experiments performed on the three heterologously expressed human nAChRs under study.

2. Structure-based design

The significance of structural water molecules in ligand protein recognition is a well-known and deeply investigated issue [34-36]. Water molecules may mediate crucial protein-protein and ligand-protein interactions as well as contribute to the favorable orientation of the ligands within the binding crevice. In a previous study, we found that the two hydroxyl-containing analogues (±)-**3** and (±)-**4** (Figure 1) perturbed the hydrogen bond network formerly present in the solvated binding cleft hosting deschloroepibatidine [31]. The theoretical binding modes were correlated with the experimental results on (±)-**3** and (±)-**4**, which, with respect to their parent compound, showed a comparable affinity at the α3β4 subtype while considerably lost affinity at the α4β2 subtype. As a consequence, the applied structural modification caused a gain of α3β4 vs α4β2 selectivity, which deserved further investigation.

Thus, we extended our study to anabaseine **2** by performing docking calculations and molecular dynamics (MD) simulations in the fully solvated α3β4 nAChR model previously developed by us [37]. Using the computational protocol applied to epibatidine **1** and deschloroepibatidine [31], we identified a plausible binding mode of **2** and then analyzed its interaction with a putative water molecule bound in the receptor area surrounded by the residues α3-Thr106, α3-Trp149 and β4-Leu119 (Figure 2A). During the MD simulations, we observed that the water molecule was firmly bound to the backbone of these residues and only occasionally interacted with the pyridine nitrogen of **2** (Figure 2B). As predicted for epibatidine **1**, in the α3β4 binding site the solvent molecules interact with the above cited receptor residues and create a hydrophilic environment which dictates the ligand orientation

[31]. In addition, to confirm the presence of the solvent molecules in the binding site, we calculated the water occupancy by the Volmap tool of VMD [38], over 50 ns of MD simulations of a solvated α3β4 model in the *apo* state. The results of this calculation suggested that the binding cleft is frequently visited by solvent molecules, as displayed by the yellow area in Figure 3.

Figures 2 and 3 to be inserted about here

Taking into account the results of our computational analysis, we designed new analogues of **2** with the aim to access the space occupied by solvent molecules. From our modeling studies (Figure 2B), we envisioned that the introduction of a benzene ring with suitable substituents at the 3-position would provide more productive interactions with the α3β4 receptor residues in the binding cleft than those afforded by the nitrogen atom of the anabaseine pyridine ring, which are presumably mediated by the water molecules bound to the backbone. By analogy with compounds (±)-**3**, (±)-**4** (Figure 1), to improve the affinity for the target subtype we initially designed and prepared the 3-hydroxybenzene **5** and 3-hydroxymethylbenzene **6** derivatives, which incorporate the hydroxyl group of the water molecule in the ligand molecular skeleton [39]. Then we synthesized the group of analogues **7-15**, to further probe the effect on the pharmacological profile of the electronic and spatial features of the 3-substituent on the aromatic ring. With the *m*-tolyl and phenyl derivatives, **7** and **8** respectively, we aimed at exploring the competitive influence of van der Waals contacts or hydrogen bonding in the interaction with the binding site. Instead, to engender stronger polar interactions within the receptor crevice, we synthesized a subgroup of 3-substituted mono-halogenated derivatives, i.e., **9** (3-F), **10** (3-Cl), **11** (3-Br), **12** (3-I), in which the progressive increase of the halogen size paralleled its electron-withdrawing properties. It is

well known that the halogen atoms can form halogen bonds with nucleophiles, e.g. electronegative atoms like oxygen, displaying a roughly linear arrangement, but also give rise to hydrogen bonds with electrophiles (H-bond donors), occurring laterally [40,41]. Halogen bonds may stabilize ligand-receptor interactions and thus positively affect the process of mutual molecular recognition. Finally, we planned the synthesis and the pharmacological evaluation of the doubly substituted congeners **13-15**.

3. Chemistry

Target compounds **5**, **6**, **10**, **12** and **13** were prepared along with a rapid synthesis of 2-substituted cyclic imines from lactams, with a reaction sequence involving the *in situ* introduction of the *N*-Boc group, an organometallic ring-opening reaction, and the nitrogen deprotection with concomitant ring-closure and dehydration [42]. As illustrated in Scheme 1, commercially available δ-valerolactam was sequentially reacted with butyllithium in THF at –78 °C, di-*tert*-butyldicarbonate and the appropriate Grignard reagent (3-methoxyphenylmagnesium bromide **16**, 3-chlorophenylmagnesium bromide **17**, 3-iodophenylmagnesium bromide **18** and 3,5-dibromophenylmagnesium bromide **19**), in turn obtained from the corresponding aryl bromide with magnesium turnings [43]. The intermediates *N*-Boc-ω-amino ketones **20-23** were treated with trifluoroacetic acid, then with 30% aqueous sodium hydroxide, providing the cyclic imines **24**, **10**, **12** and **13**, respectively [42].

Scheme 1 to be inserted about here

Demethylation of derivative **24** with concentrated hydrobromic acid afforded the desired

final compound **5**. On the other hand, the synthesis of **6** took advantage of a microwave-mediated fast carbonylation of aryl iodide **12**, using molybdenum hexacarbonyl as a solid carbon monoxide source [44] to provide the corresponding methyl ester **25**. Red-Al® reduction [45] of the latter produced the related hydroxymethylbenzene cyclic imine **6**.

In a parallel way, cyclic imines **7**-**9**, **11**, **14** and **15** were synthesized utilizing the commercially available 5-bromovaleronitrile as the key intermediate (Scheme 2). The *m*-tolyl derivative **7** was prepared transforming 3-bromotoluene into the corresponding *m*-tolylmagnesium bromide **26** [43], which was reacted with 5-bromovaleronitrile in a tandem addition-cyclization reaction at room temperature in tetrahydrofuran to give the desired compound [46]. Alternatively, 5-bromovaleronitrile was coupled and cyclized with organolithiums [47]. Indeed, compounds **8**, **9**, **11** and **14** were synthesized by reaction of 5-bromovaleronitrile, respectively, with commercially available phenyllithium **27** or (3-fluorophenyl)lithium **28**, (3-bromophenyl)lithium **29** and (3-bromo-5-fluorophenyl)lithium **30**, which were in turn prepared from precursor bromophenyl derivatives by treatment with 1.6 M *n*-butyllithium in hexane [48].

According to the protocol applied to **12** (Scheme 1), the cyclic 3-bromo-5-fluorophenyl imine **14** was converted into the corresponding methyl ester **31**, which was reduced to the desired hydroxymethyl derivative **15**. At last, the target compounds **5**-**15** were converted into their corresponding hydrochlorides by treatment with a 4.0 M hydrochloric acid solution in 1,4-dioxane.

Scheme 2 to be inserted about here

3. Pharmacology

3.1. Binding studies

As detailed in Table 1, the new compounds as well as the reference ligand **2** were tested for their ability to compete with [^{3}H]epibatidine for binding to heterologously expressed human α3β4 and rat α4β2 nAChRs. The target derivatives were also assayed at the rat hippocampal α7 nAChR subtype, using [^{125}I]α-bungarotoxin as radioligand.

It is worth remarking that replacement of the pyridine nucleus of anabaseine **2** with the 3-hydroxybenzene and 3-hydroxymethylbenzene moieties to give **5** and **6** caused, in terms of binding affinity, a 500-fold reduction at the α4β2 subtype, and, at least for **5**, a 300-fold decrease at the α7 subtype. On the other hand, the new compounds exhibited a moderately lower (K_i = 680 nM for **5**) or a slightly higher (K_i = 80 nM for **6**) affinity than **2** (K_i = 107 nM) at the α3β4 nAChR. Moreover, the affinity of the anabaseine-related ligand **6** at the latter subtype matched that of the two epibatidine-related analogues (±)-**3** and (±)-**4**, with an additional, remarkable gain (438-fold) of α3β4 over α4β2 subtype selectivity.

Table 1 to be inserted about here

As shown in Table 1, when the *m*-hydroxymethyl group of **6** was replaced by a lipophilic moiety (CH_3, compound **7**) or a hydrogen atom (compound **8**), an almost complete loss of α3β4 vs α4β2 selectivity was observed, mainly due to a partial increase of affinity for the α4β2 subtype. The 3-halogen derivatives **9**-**12**, synthesized to ascertain the importance of the polar halogen bond interactions in the binding site, indeed exhibited from high to low nanomolar binding affinities at α3β4 and α7 nAChRs, and the related K_i values gradually decreased at both receptor subtypes with increasing the size of the halogen substituent. Compound **12**, carrying the largest 3-iodo atom, showed the highest affinity for α3β4 and α7

nAChRs, with K_i values of 4.7 nM and 11.3 nM, respectively. In addition, this derivative had the highest value of α3β4 vs α4β2 selectivity (806-fold) in the series. The introduction of a second bromine atom on the 5 position of the phenyl ring in compound **11** led to the dibromo analogue **13**, which showed a moderate decrease of binding affinity at α3β4 and a more significant one at α4β2 and α7 nAChRs, thereby increasing subtype selectivity respect to the monobromo congener. Conversely, the presence of the additional 5-F (compounds **14** and **15**) had only a negligible or modest effect on the affinity at α3β4 and α7 subtypes relative to the corresponding mono-substituted derivatives **11** and **6**, respectively. However, compound **15** exhibited a 47-fold lower K_i value than that found for its analogue **6** at the heteromeric α4β2 nAChRs, suggesting a different binding mode of the two ligands with a concomitant drop in subtype selectivity.

Together, the modified anabaseine derivatives **5-15** bearing different *meta* substituents on the benzene ring behaved as good to excellent α3β4 ligands with a poor α3β4 vs α7 selectivity. In this set of compounds, the introduction of heavier halogen atoms on the same 3-position, on one hand caused a clear, comparable increase of both α3β4 and α7 affinity, on the other amplified the ability of the ligands to distinguish the α3β4 from the α4β2 heteromeric nAChRs.

3.2. Electrophysiological experiments

Based on the above discussed binding data, derivatives **6**, **12** and **13** are among the analogues with the highest affinity for the α3β4 nAChR subtype (K_i = 80, 4.7 and 70.8 nM, respectively) and possess the highest values (438, 806 and 266, respectively) of α3β4 vs α4β2 selectivity. Thus, these ligands were selected for evaluation of their functional activity

at the human α3β4, α4β2 and α7 nAChR subtypes heterologously expressed in the rat anterior pituitary GH4C1 cell line. The functional expression of the different nAChRs was evaluated by measuring the whole-cell inward current elicited by ACh 1 mM, with mean current amplitudes of 3.5 ± 0.5 nA, 1.1 ± 0.2 nA and 0.7 ± 0.1 nA for α3β4 (n=36), α4β2 (n=27) and α7 (n=22), respectively.

As depicted in Figure 4A, the 3-hydroxymethylbenzene derivative **6** elicited significant inward currents when applied on GH4C1 cells expressing α3β4 and α7 nAChRs, while its action on α4β2 nAChRs was completely absent. In particular, the analysis of the dose-response relationships disclosed EC_{50} values of 20.0 μM and 59.7 μM at α3β4 and α7 nAChRs, respectively. These results are comparable to those found for the epibatidine-related derivative (±)-**3**, which showed a similar activation pattern [31], and indicate that **6** behaves as a partial agonist at α3β4 and as a full agonist at α7 nAChRs. Replacement of the CH_2OH group of **6** with iodine gave **12**, which exhibited the highest binding affinity at α3β4 nAChRs and the most pronounced α3β4 over α4β2 selectivity. In addition, compound **12** was a partial agonist at α3β4 nAChRs displaying higher potency and efficacy than its analogue **6**, with an EC_{50} value of 7.4 μM and a maximal current reaching 60% of that evoked by ACh (Figure 4B). Furthermore, **12** had significantly lower efficacy and potency at α7 nAChRs and no effect at α4β2 nAChRs (Figure 4B), thus evidencing a good functional selectivity at the investigated subtypes. The functional profiles of compounds **6** and **12** showed a trend consistent with the outcome of the binding assays (Table 1). However, for the 3,5-dibromo derivative **13**, characterized by rather different binding affinity values [K_i: 70.8 nM (α3β4), 343 nM (α7), 18.8 μM (α4β2)], an almost complete lack of response was observed in electrophysiological experiments at the three studied subtypes (Figure 4C). This result

strongly recalls the complex relationships between the gating properties of a ligand and its binding affinity for a given receptor channel [49]. Furthermore, both **12** and **13** exhibited negligible effects when assayed as antagonists of heteromeric nAChRs (data not shown). Thus, considering the above discussed electrophysiological data, **12** behaves as an interesting α3β4 partial agonist with a very high binding/functional selectivity over the α4β2 subtype as well as a pronounced functional selectivity over the α7 subtype.

Figure 4 to be inserted about here

4. Docking and Molecular Dynamics analysis

It is worth noting that, in the subset of derivatives **8**-**12**, the overall poor α4β2 binding affinity was slightly affected by the nature of the substituent on the 3-position of the benzene ring. Conversely, as previously discussed, a gradual enhancement of the affinity was observed on passing from the unsubstituted derivative **8** (K_i = 194 nM) to the 3-iodo analogue **12** (K_i = 4.7 nM) at the α3β4 subtype. A parallel trend characterized the affinity of the same compounds at the α7 subtype (from K_i = 2400 nM for **8** to K_i = 11.3 nM for **12**). This may be due to the presence of a highly conserved sub-area in the two nAChR proteins involved in the ligand-receptor interactions. To shed light on this speculation, we performed docking and MD simulations on the most interesting compound **12** within the α3β4 nAChR binding site. As shown in Figure 5, the docking studies revealed that the protonated nitrogen of the cyclic imine ring of **12** is ideally positioned to generate a stabilizing H-bonding interaction with the carbonyl oxygen of α3-Trp149 and a cation-π interaction with the side chain of the same residue. Moreover, the ligand aryl moiety was projected under loop-C toward the same zone

previously occupied by the pyridine nitrogen of anabaseine and, noteworthy, the iodine atom was able to interact with the protein area in which solvent molecules are expected to be present, close to β4-Leu119 and α3-Ser150 residues (Leu119 and Ser149 in the α7 sequence, respectively). Most striking is the observation that the side chain of β4-Arg79 was in close proximity to the halogen atom, creating a good environment for the acceptance of heavy and electron-rich atoms like iodine. This hypothetical binding mode likely accounts for the enhanced affinity associated with the increased size and volume of the halogen atom in compounds **9**-**12**.

The same Arg79 was found in the α7 and β2 sequences, but in our α4β2 model it was differently oriented at the end of the MD equilibration. Indeed, being involved in a salt bridge with the side chain of α4-Glu193, this residue was unavailable for interacting with ligand molecules in the orthosteric site. Moreover, the α3-Ser150 residue corresponds to a threonine in the α4 sequence (α4-Thr148), and the presence of an additional methyl group in the side chain should significantly hamper the acceptance of large atoms. This indicates a restrictive size limitation for the substituents on the phenyl ring and justifies the overall low affinity of the compounds **8**-**12** at the α4β2 nAChR subtype.

Figure 5 to be inserted about here

The crucial role of the halogen atom in the ligand-receptor interaction can be evaluated by comparing the binding affinities of the newly synthesized compounds **7** and **12**. Indeed, the anabaseine-related derivative **12** (3-I) showed a 33-fold higher affinity for the α3β4 subtype than its analog **7** (3-CH_3). As a matter of fact, the two compounds differ only for the substituent in position 3 of the phenyl ring, from iodine to methyl, which have similar van der Waals radii (close to 2 Å) but show relevant differences in terms of electronegativity, electron

density and capability to accept hydrogen bonds. This clearly suggests that the most suitable interaction of the ligands in the α3β4 receptor binding pocket should be lipophilic as well as polar in nature. The same conclusions can be drawn if the binding data on the α7 nAChR are taken into account, since, quite similarly, the iodinated derivative **12** displayed a 34-fold higher affinity than the methyl-substituted derivative **7** at this subtype.

In an attempt to rationalize the low biological activity of the 3,5-dibromo derivative **13** at the α3β4 nAChR subtype, further docking and MD simulations were performed. The results highlighted that the binding mode of **13** was not dissimilar from that predicted for the 3-iodo analogue **12**, but the presence of an additional halogen atom in 5 led to a different induced-fit effect in the receptor binding cleft upon MD simulations. Indeed, whereas **12** did not essentially alter the distance between loop C and the α3-Ser150, at the end of simulations the 3,5-dibromo compound **13** increased the same distance by 3 Å. This computational evidence could account for the different electrophysiological profile of **13**, which lost the agonist activity shown by its analogue **12** at the α3β4 nAChR subtype.

The role exerted by loop C in modulating the permeability of nicotinic channels is still debated. Recently, X-ray crystal structures of nicotine analogues, endowed with functional profiles spanning from agonists to antagonists within the LBD of *Limnea S.*, were reported in the PDB [50]. The authors concluded that the loop C conformation is not directly involved in the functional profile shown by the ligands. Nevertheless, a direct connection between the bulkiness of orthosteric ligands and the capacity to limit the opening of the channel exists. In this respect, Hansen et al. [25] suggested that the loop C extension and closure might be the distinguishing feature between complexes of the nAChR with agonists and antagonists. On the other hand, Mukhtasimova et al. [51] proposed that some key interactions between residues belonging to loop C are required to efficiently modulate the channel-gating

equilibrium. Our data suggest that a combined ligand interaction with the loop C and the alpha subunit counterpart may control the functional response of the nicotinic channel.

5. Conclusion

The α3β4 nAChR, mainly expressed in the in sensory and autonomic ganglia and in the adrenal gland, is frequently referred to as the "ganglionic nAChR". Recent studies have provided compelling evidence that the α3β4* nAChRs present in the MHb-IPN brain pathway regulate nicotine reinforcement, dependence and withdrawal [52,19,53]. Injection of α3β4 nicotinic receptor antagonists into the MHb decreases self-administration of multiple abused drugs, including nicotine, morphine, cocaine and alcohol [54]. Due to desensitization of α3β4 nAChRs, even the high affinity α3β4 selective partial agonist AT-1001 was found to block nicotine self-administration and relapse-like behavior in rats [55], thus making this compound a potentially safer and clinically useful agent for smoking cessation.

The goal of the present study was to identify and characterize new α3β4 selective ligands aiming at new compounds for smoking cessation and/or to treat lung cancers expressing a high level of the mRNAs for the α3 and β4 subunits. To this end, we initially performed an MD theoretical investigation on the natural nicotinic agonist anabaseine **2** within the α3β4 binding cleft. This analysis highlighted that water molecules may generate H-bond interactions with complementary residues of the surrounding receptor protein, thus favoring a proper orientation of the ligand. To learn more about the structural determinants which bring about a gain in α3β4 nAChR subtype selectivity, at first we chose to modify the structure of **2** by replacing its 3-pyridinyl moiety with the 3-OH or the 3-CH_2OH benzene ring (compounds **5** and **6**, respectively), then the set of investigated derivatives was extended to the 3-mono- or

3,5-disubstituted analogs **7-15**.

The novel compounds behaved as good to high affinity α3β4 subtype ligands [K_i values from 680 nM for **5** to 4.7 nM for **12**] and, in some instances, a noteworthy α3β4 vs α4β2 selectivity was observed (i.e., 438-fold for **6** and 806-fold for **12**). Remarkably, in the subgroup of 3-halogen-phenyl analogues **9-12**, the α3β4 affinity progressively increased with the size of the substituent, highlighting a critical contribution of halogen bonding in the process of recognition by the α3β4 subtype. Computational studies confirmed that, in the binding crevice of the α3β4 receptor, a favorable sub-area is available for the acceptance of heavy and electron-rich atoms like halogens. We hypothesized the presence of a similar conserved sub-area also within the binding site of the α7 receptor, since the same derivatives **9-12** showed a quite comparable affinity trend, which precluded their ability to discriminate between the heteromeric α3β4 and the homomeric α7 subtype.

Finally, three relevant α3β4 ligands were further assessed in electrophysiological experiments. This analysis indicated that the 3-iodo-substituted derivative **12** stands out as a high affinity α3β4 nAChR partial agonist, which couples a very high α3β4 vs α4β2 selectivity with a selective activation of the α3β4-mediated functional response. In summary, inspired by the structural skeleton of anabaseine, we successfully identified a position on the benzene ring of a small set of new analogs which is crucial in triggering a gain in both α3β4 affinity and binding/functional selectivity.

6. Experimental protocols

6.1. Chemistry

6.1.1. General methods

^{1}H NMR and ^{13}C NMR spectra were recorded with a Varian Mercury 300 (^{1}H, 300.063; ^{13}C, 75.451 MHz) spectrometer in $CDCl_3$ solutions (unless otherwise indicated) at 20 °C. Chemical shifts (δ) are expressed in ppm and coupling constants (J) in Hz. TLC analyses were performed on commercial silica gel 60 F_{254} aluminum sheets; spots were further evidenced by spraying with a dilute alkaline potassium permanganate solution or a phosphomolybdic acid solution and, for tertiary amines, with the Dragendorff reagent. All microwave irradiation experiments were carried out in a CEM Discover SP microwave apparatus, operating at a frequency of 2.45 GHz with continuous irradiation power from zero to 300W, utilizing the standard absorbance level of 50W maximum power. The reactions were performed in a standard pressurized 10 mL reaction vessel, sealed with Teflon septum and placed in the microwave cavity. The reaction was irradiated at a required ceiling temperature using maximum power for the stipulated time. Then it was cooled to 40 °C with gas jet cooling. Melting points were determined on a model B 540 Büchi apparatus and are uncorrected. ESI mass spectra were obtained on a Varian 320 LC-MS/MS instrument. Data are reported as mass-to-charge ratio (m/z) of the corresponding positively charged molecular ions. Microanalyses (C, H, N) agreed with the theoretical value within ± 0.4%. Compound **27** and all other reagents and solvents were purchased from Sigma-Aldrich Srl (Milan, Italy) and used without further purification. Anabaseine dihydrochloride was prepared according to a known procedure [56].

*6.1.2. Synthesis of target compounds **5**, **6**, **10**, **12** and **13***

*6.1.2.1. tert-Butyl 5-(3-methoxyphenyl)-5-oxopentylcarbamate (**20**)*

To a solution of δ-valerolactam (1 g, 10.10 mmol) in anhydrous THF (27 mL) at –78 °C under an argon atmosphere was added dropwise 2.5 M butyllithium in hexanes (4.04 mL,

10.09 mmol) and after 30 min of stirring, a solution of di-*tert*-butyldicarbonate (2.2 g, 10.10 mmol) in anhydrous THF (3.5 mL) was added and temperature was maintained at –78 °C for 3 h. Then a solution of 3-methoxyphenylmagnesium bromide **16**, prepared from 2.45 g of 3-bromoanisole and 368 mg of magnesium turnings in anhydrous THF (14 mL), was added and stirring was continued at the same temperature for further 3 h. The reaction was allowed to warm to room temperature and quenched with 2.0 M HCl (10 mL). The mixture was extracted with diethyl ether (3 × 15 mL) and the combined organic layers were washed with a 5% $NaHCO_3$ aqueous solution (1 × 20 mL) and brine (1 × 20 mL), dried over anhydrous sodium sulphate and concentrated in vacuo to obtain **20** as a yellow oil (2.84 g, 92% yield). R_f = 0.21 (cyclohexane/ethyl acetate 9:1). ^{1}H NMR: δ 1.43 (s, 9H), 1.51–1.61 (m, 2H), 1.70–1.81 (m, 2H), 2.97 (t, J = 7.2 Hz, 2H), 3.14 (t, J = 6.4 Hz, 2H), 3.84 (s, 3H), 4.63 (br s, 1H), 7.09 (ddd, J = 8.3, 2.8, 1.1 Hz, 1H), 7.35 (t, J = 8.3 Hz, 1H), 7.46–7.47 (m, 1H), 7.50–7.53 (m, 1H). ^{13}C NMR: δ 21.2, 28.4 (3C), 29.4, 38.4, 40.0, 55.8, 79.5, 115.9, 118.7, 122.1, 129.3, 138.9, 155.9, 160.5, 185.1. MS (ESI) *m/z* $[M+H]^+$ Calcd for $C_{17}H_{26}NO_4^+$: 308.19. Found: 308.2.

*6.1.2.2. tert-Butyl 5-(3-Chlorophenyl)-5-oxopentylcarbamate (**21**)*

The title compound was obtained according to the method described for compound **20** by employing δ-valerolactam (992 mg, 10.0 mmol) and 3-chlorophenylmagnesium bromide **17** prepared by treatment of 1-bromo-3-chlorobenzene (1.2 mL, 10.00 mmol) with magnesium turnings (243 mg) to afford **21** as a dark yellow oil (1.44 g, 46% yield). R_f = 0.28 (cyclohexane/ethyl acetate 4:1). ^{1}H NMR: δ 1.41 (s, 9H), 1.49–1.62 (m, 2H), 1.69–1.79 (m, 2H), 2.95 (t, J = 7.2 Hz, 2H), 3.13 (t, J = 6.9 Hz, 2H), 4.64 (br s, 1H), 7.37 (t, J = 7.8 Hz, 1H), 7.48–7.52 (m, 1H), 7.78–7.82 (m, 1H), 7.89 (t, J = 1.7 Hz, 1H). ^{13}C NMR: δ 21.3, 28.6 (3C),

29.8, 38.3, 40.4, 79.4, 126.3, 128.4, 130.2, 133.2, 135.2, 138.6, 156.2, 198.9. MS (ESI) *m/z* $[M+H]^+$ Calcd for $C_{16}H_{23}ClNO_3^+$: 312.14. Found: 312.1.

*6.1.2.3. tert-Butyl 5-(3-iodophenyl)-5-oxopentylcarbamate (**22**)*

The title compound was obtained according to the method described for compound **20** by employing *δ*-valerolactam (1 g, 10.10 mmol) and 3-iodophenylmagnesium bromide **18** prepared by treatment of 3-bromoiodobenzene (1.67 mL, 13.11 mmol) with magnesium turnings (368 mg) to afford **22** as a yellow oil (2.72 g, 67% yield). R_f = 0.32 (cyclohexane/ethyl acetate 4:1). ^{1}H NMR: δ 1.44 (s, 9H), 1.52–1.65 (m, 2H), 1.72–1.83 (m, 2H), 2.98 (t, J = 7.2 Hz, 2H), 3.16 (t, J = 6.3 Hz, 2H), 4.58 (br s, 1H), 7.23–7.29 (m, 1H), 7.44 (dt, J = 8.0, 5.8 Hz, 1H), 7.61–7.65 (m, 1H), 7.71–7.75 (m, 1H). ^{13}C NMR: δ 21.2, 28.6 (3C), 29.5, 38.4, 40.6, 79.5, 124.5, 127.7, 130.1, 133.8, 136.1, 138.7, 155.1, 199.2. MS (ESI) *m/z* $[M+H]^+$ Calcd for $C_{16}H_{23}INO_3^+$: 404.07. Found: 404.1.

*6.1.2.4. tert-Butyl 5-(3,5-dibromophenyl)-5-oxopentylcarbamate (**23**)*

The title compound was obtained according to the method described for compound **20** by employing *δ*-valerolactam (1.24 g, 12.50 mmol) and 3,5-dibromophenylmagnesium bromide **19** prepared by treatment of 1,3,5-tribromobenzene (3.94 g, 12.50 mmol) with magnesium turnings (304 mg) to afford **23** as a yellow oil (2.01 g, 37% yield). R_f = 0.41 (cyclohexane/ethyl acetate 4:1). ^{1}H NMR: δ 1.42 (s, 9H), 1.47–1.62 (m, 2H), 1.71–1.78 (m, 2H), 2.93 (t, J = 7.2 Hz, 2H), 3.05–3.20 (m, 2H), 4.62 (br s, 1H), 7.81 (t, J = 1.6 Hz, 1H), 7.97 (d, J = 1.6 Hz, 2H). ^{13}C NMR: δ 21.4, 28.7 (3C), 29.6, 38.2, 40.3, 79.4, 123.3 (2C), 128.6 (2C), 133.7, 139.5, 156.1, 198.7. MS (ESI) *m/z* $[M+H]^+$ Calcd for $C_{16}H_{22}Br_2NO_3^+$: 434.00. Found: 434.0.

*6.1.2.5. 6-(3-Methoxyphenyl)-2,3,4,5-tetrahydropyridine (**24**)*

Trifluoroacetic acid (7 mL) was added dropwise at 0 °C to compound **20** (2.74 g, 8.90 mmol) and then stirring was continued at room temperature for 3 h. After completion of the reaction, the mixture was cooled to 0 °C and quenched by dropwise addition of 30% NaOH aqueous solution until pH 10-11 and then extracted with diethyl ether (5 × 20 mL). The combined organic layers were washed with brine (1 × 60 mL), dried over anhydrous sodium sulphate and concentrated in vacuo to obtain **24** as a yellow oil (1.20 g, 71% yield). R_f = 0.22 (cyclohexane/ethyl acetate 9:1). ^{1}H NMR: δ 1.64–1.71 (m, 2H), 1.79–1.88 (m, 2H), 2.60–2.66 (m, 2H), 3.81–3.86 (m, 2H), 3.84 (s, 3H), 6.94 (ddd, J = 7.7, 2.8, 1.7 Hz, 1H), 7.25–7.31 (m, 2H), 7.37–7.38 (m, 1H). ^{13}C NMR: δ 19.9, 22.0, 27.4, 50.0, 55.6, 111.0, 116.2, 118.7, 129.4, 141.7, 159.9, 166.1. MS (ESI) *m/z* $[M+H]^+$ Calcd for $C_{12}H_{16}NO^+$: 190.12. Found: 190.1.

*6.1.2.6. 6-(3-Chlorophenyl)-2,3,4,5-tetrahydropyridine (**10**)*

Reaction of compound **21** (1.10 g, 3.53 mmol) with trifluoroacetic acid as described for the synthesis of **24** gave compound **10** as a yellow oil (612 mg, 90% yield). R_f = 0.34 (cyclohexane/ethyl acetate 4:1). ^{1}H NMR: δ 1.58–1.65 (m, 2H), 1.73–1.82 (m, 2H), 2.49–2.55 (m, 2H), 3.78–3.82 (m, 2H), 7.22–7.31 (m, 2H), 7.56–7.59 (m, 1H), 7.74–7.75 (m, 1H). ^{13}C NMR: δ 19.8, 22.0, 27.1, 50.2, 124.2, 126.4, 129.6 (2C), 134.6, 142.1, 164.4. MS (ESI) *m/z* $[M+H]^+$ Calcd for $C_{11}H_{13}ClN^+$: 194.07. Found: 194.1.

*6.1.2.7. 6-(3-Iodophenyl)-2,3,4,5-tetrahydropyridine (**12**)*

Reaction of compound **22** (2.60 g, 6.45 mmol) with trifluoroacetic acid as described for the synthesis of **24** gave compound **12** as a yellow oil (1.62 g, 88% yield). R_f = 0.38 (cyclohexane/ethyl acetate 4:1). ^{1}H NMR: δ 1.63–1.71 (m, 2H), 1.80–1.88 (m, 2H), 2.55–2.61

(m, 2H), 3.82–3.86 (m, 2H), 7.10 (t, J = 7.8 Hz, 1H), 7.21–7.26 (m, 1H), 7.48–7.52 (m, 1H), 7.66–7.62 (m, 1H). ^{13}C NMR: δ 19.8, 22.0, 27.2, 50.2, 122.9, 124.7, 129.4, 132.6, 138.6, 142.4, 164.2. MS (ESI) *m/z* $[M+H]^+$ Calcd for $C_{11}H_{13}IN^+$: 286.01. Found: 286.0.

*6.1.2.8. 6-(3,5-Dibromophenyl)-2,3,4,5-tetrahydropyridine (**13**)*

Reaction of compound **23** (1.80 g, 4.14 mmol) with trifluoroacetic acid as described for the synthesis of **24** gave compound **13** as a yellow oil (591 mg, 45% yield). R_f = 0.66 (cyclohexane/ethyl acetate 4:1). ^{1}H NMR: δ 1.57–1.63 (m, 2H), 1.73–1.78 (m, 2H), 2.44–2.49 (m, 2H), 3.75–3.79 (m, 2H), 7.58 (t, J = 1.8 Hz, 1H), 7.79 (d, J = 1.8 Hz, 2H). ^{13}C NMR: δ 19.7, 21.9, 27.2, 50.3, 123.2 (2C), 128.1 (2C), 134.9, 143.6, 163.3. MS (ESI) *m/z* $[M+H]^+$ Calcd for $C_{11}H_{12}Br_2N^+$: 315.93. Found: 316.0.

*6.1.2.9. 3-(3,4,5,6-Tetrahydropyridin-2-yl)phenol (**5**)*

A solution of compound **24** (201 mg, 1.06 mmol) in 48% aqueous HBr (3 mL) was stirred under refluxing conditions for 6 h and then was cooled to room temperature and stirring was continued overnight. The reaction mixture was concentrated under vacuum, the residue was adjusted to pH 11 with a saturated aqueous solution of sodium hydrogen carbonate and then extracted with ethyl acetate (5 × 20 mL). The combined organic layers were washed with brine (1 × 50 mL), dried over anhydrous sodium sulphate, filtered and concentrated under reduced pressure to obtain compound **5** as a yellow oil (147 mg, 79% yield). R_f = 0.33 (dichloromethane/methanol 9:1). ^{1}H NMR: δ 1.66–1.73 (m, 2H), 1.78–1.86 (m, 2H), 2.59–2.63 (m, 2H), 3.77–3.81 (m, 2H), 6.81–6.85 (m, 1H), 7.09–7.19 (m, 2H), 7.25–7.26 (m, 1H). ^{13}C NMR: δ 19.6, 21.7, 28.0, 49.1, 113.9, 117.9, 118.2, 129.7, 140.8, 157.3, 169.4. MS (ESI) *m/z* $[M+H]^+$ Calcd for $C_{11}H_{14}NO^+$: 176.11. Found: 176.2.

*6.1.2.10. Methyl-3-(3,4,5,6-tetrahydropyridin-2-yl)benzoate (**25**)*

To a solution of **12** (1.2 g, 4.21 mmol) in dioxane (4.5 mL), molybdenum hexacarbonyl (1.67 g, 6.32 mmol), 10% palladium on activated charcoal (200 mg), 4-(dimethylamino)pyridine (1.03 g, 8.42 mmol), *N*,*N*-diisopropylethylamine (1.09 g, 8.42 mmol) and methanol (1.7 mL, 42.10 mmol) were added and the mixture was sealed and heated in a microwave reactor at 130°C using 50 W for 35 minutes (2 cycles). The reaction mixture was filtered over a Celite® pad and the filtrate was concentrated under reduced pressure. The residue was then taken up with a saturated aqueous solution of $NaHCO_3$ (15 mL) and extracted with ethyl acetate (3 × 10 mL). The combined organic layers were washed with brine (1 × 15 mL), dried over anhydrous sodium sulphate, filtered and concentrated under reduced pressure to afford a crude mixture which was purified by silica gel column chromatography (cyclohexane/ethyl acetate 85:15). The methyl ester intermediate **25** was obtained as a yellow oil (400 mg, 44% yield). R_f = 0.3 (cyclohexane/ethyl acetate 7:3). ^{1}H NMR: δ 1.64–1.72 (m, 2H), 1.81–1.89 (m, 2H), 2.62–2.69 (m, 2H), 3.81–3.88 (m, 2H), 3.91 (s, 3H), 7.44 (t, J = 7.7 Hz, 1H), 7.99 (dd, J = 7.7, 1.9 Hz, 1H), 8.04 (d, J = 7.7 Hz, 1H), 8.38 (d, J = 1.9 Hz, 1H). ^{13}C NMR: δ 19.8, 22.0, 27.3, 50.2, 53.4, 126.2, 127.3, 128.6, 130.6, 130.8, 140.7, 165.2, 166.2. MS (ESI) *m/z* $[M+H]^+$ Calcd for $C_{13}H_{16}NO_2^+$: 218.12. Found: 218.1.

*6.1.2.11. (3-(3,4,5,6-Tetrahydropyridin-2-yl)phenyl)methanol (**6**)*

To a solution of **25** (400 mg, 1.84 mmol) in anhydrous THF (37 mL) under inert atmosphere was added Red-Al 65% in toluene (2.4 mL, 7.73 mmol) and the mixture was stirred for 1 h at room temperature. Then, a saturated aqueous solution of $NaHCO_3$ (10 mL)

was added to the reaction and the mixture was extracted with ethyl acetate (3 × 10 mL). The combined organic layers were dried over anhydrous sodium sulphate, filtered and concentrated under reduced pressure. The crude residue was purified by silica gel column chromatography (ethyl acetate) to provide the alcohol derivative **6** as a yellow oil (178 mg, 51% yield). R_f = 0.41 (dichloromethane/methanol 85:15). ^{1}H NMR: δ 1.64–1.73 (m, 2H), 1.75 (br s, 1H), 1.77–1.88 (m, 2H), 2.60–2.65 (m, 2H), 3.81–3.86 (m, 2H), 4.71 (s, 2H), 7.34–7.38 (m, 2H), 7.63–7.66 (m, 1H), 7.76–7.77 (m, 1H). ^{13}C NMR: δ 19.6, 22.6, 27.1, 49.8, 64.6, 126.8, 127.1, 128.8, 129.1, 140.8, 142.8, 168.2. MS (ESI) *m/z* $[M+H]^+$ Calcd for $C_{12}H_{16}NO^+$: 190.12. Found: 190.1.

*6.1.3. Synthesis of target compounds **7**, **8**, **9**, **11**, **14** and **15***

6.1.3.1. 6-m-Tolyl-2,3,4,5-tetrahydropyridine (7)

A solution of *m*-tolylmagnesium bromide **26**, prepared from 416 µL of 3-bromotoluene and 83 mg of magnesium turnings in anhydrous THF (3 mL), was added dropwise under inert atmosphere to a solution of 5-bromovaleronitrile (400 µL, 3.43 mmol) in anhydrous THF (3 mL). The mixture was stirred at room temperature for 1 h, quenched with a saturated aqueous solution of $NaHCO_3$ (3 mL) and extracted with dichloromethane (3 × 10 mL). The combined organic layers were dried over anhydrous sodium sulphate, filtered and concentrated under reduced pressure. The crude residue was purified by silica gel column chromatography (dichloromethane/methanol 95:5) to provide the compound **7** as a yellow oil (225 mg, 38% yield). R_f = 0.40 (dichloromethane/methanol 95:5). ^{1}H NMR: δ 1.63–1.71 (m, 2H), 1.79–1.87 (m, 2H), 2.37 (s, 3H), 2.60–2.66 (m, 2H), 3.80–3.86 (m, 2H), 7.18–7.29 (m, 2H), 7.51–7.54 (m, 1H), 7.61–7.62 (m, 1H). ^{13}C NMR: δ 20.0, 21.7, 22.1, 27.4, 50.1, 123.3, 126.8, 128.3, 130.5, 138.1, 140.4, 166.2. MS (ESI) *m/z* $[M+H]^+$ Calcd for $C_{12}H_{16}N^+$: 174.13. Found: 174.2.

*6.1.3.2. 6-Phenyl-2,3,4,5-tetrahydropyridine (**8**)*

The title compound was obtained according to the method described for compound **7** by dropwise addition of a 1.8 M phenyllithium solution of **27** (914 μL, 1.65 mmol) in dibutyl ether to 5-bromovaleronitrile (170 μL, 1.46 mmol) in anhydrous THF (2.5 mL) under inert atmosphere. The mixture was refluxed for 3 h and after the usual work-up the crude residue was purified by silica gel column chromatography (dichloromethane/methanol 95:5) to provide **8** as a yellow oil (197 mg, 85% yield). R_f = 0.32 (dichloromethane/methanol 95:5). ^{1}H NMR: δ 1.63–1.71 (m, 2H), 1.79–1.88 (m, 2H), 2.60–2.66 (m, 2H), 3.81–3.86 (m, 2H), 7.36–7.39 (m, 3H), 7.75–7.78 (m, 2H). ^{13}C NMR: δ 20.0, 22.1, 27.3, 50.2, 126.1 (2C), 128.4 (2C), 129.7, 140.5, 165.8. MS (ESI) *m/z* $[M+H]^+$ Calcd for $C_{11}H_{14}N^+$: 160.11. Found: 160.2.

*6.1.3.3. 6-(3-Fluorophenyl)-2,3,4,5-tetrahydropyridine (**9**)*

The title compound was obtained according to the method described for compound **7**. (3-Fluorophenyl)lithium **28** was prepared by dropwise addition of 1.6 M *n*-butyllithium (1.40 mL) in hexanes to 1-bromo-3-fluorobenzene (259 μL, 2.32 mmol) in anhydrous diethyl ether (2.5 mL) at –78 °C. After stirring for 1 h at the same temperature, the reaction mixture was slowly cannulated into a flask containing a solution of 5-bromovaleronitrile (200 μL, 1.72 mmol) in anhydrous THF (2.5 mL) and stirred at room temperature for 12 h. After the usual work-up, the crude residue was purified by silica gel column chromatography (dichloromethane/methanol 95:5) to provide **9** as a light yellow oil (82 mg, 27% yield). R_f = 0.31 (dichloromethane/methanol 95:5). ^{1}H NMR: δ 1.62–1.70 (m, 2H), 1.78–1.86 (m, 2H), 2.55–2.60 (m, 2H), 3.80–3.85 (m, 2H), 7.02–7.09 (m, 1H), 7.26–7.35 (m, 1H), 7.45–7.52 (m, 2H). ^{13}C NMR: δ 19.9, 22.0, 27.3, 50.1, 113.1 (d, J = 22.5 Hz), 116.5 (d, J = 21.3 Hz), 121.7

(d, J = 2.6 Hz), 129.8 (d, J = 8.0 Hz), 142.8, 163.1 (d, J = 244.0 Hz), 164.8. MS (ESI) *m/z* $[M+H]^+$ Calcd for $C_{11}H_{13}FN^+$: 178.10. Found: 178.3.

*6.1.3.4. 6-(3-Bromophenyl)-2,3,4,5-tetrahydropyridine (**11**)*

The title compound was obtained according to the method described for compound **7**. (3-Bromophenyl)lithium **29** was prepared by addition of 1.6 M *n*-butyllithium (1.40 mL) in hexanes to 1,3-dibromobenzene (280 µL, 2.32 mmol) in anhydrous diethyl ether (2.5 mL) at –78 °C. After stirring for 1 h at the same temperature, the reaction mixture was slowly cannulated into a flask containing a solution of 5-bromovaleronitrile (200 µL, 1.72 mmol) in anhydrous THF (2.5 mL) and stirred at room temperature for 12 h. After the usual work-up, the crude residue was purified by silica gel column chromatography (dichloromethane/methanol 98:2) to provide **11** as a yellow oil (129 mg, 32% yield). R_f = 0.30 (dichloromethane/methanol 98:2). ^{1}H NMR: δ 1.61–1.69 (m, 2H), 1.77–1.86 (m, 2H), 2.53–2.59 (m, 2H), 3.79–3.85 (m, 2H), 7.22 (t, J = 8.0 Hz, 1H), 7.48 (ddd, J = 8.0, 1.9, 0.8 Hz, 1H), 7.64–7.67 (m, 1H), 7.92 (t, J = 1.9 Hz, 1H). ^{13}C NMR: δ 19.8, 22.0, 27.2, 50.2, 122.9, 124.7, 129.3, 130.0, 132.6, 142.3, 164.6. MS (ESI) *m/z* $[M+H]^+$ Calcd for $C_{11}H_{13}BrN^+$: 238.02. Found: 238.2.

*6.1.3.5. 6-(3-Bromo-5-fluorophenyl)-2,3,4,5-tetrahydropyridine (**14**)*

The title compound was obtained according to the method described for compound **7**. (3-Bromo-5-fluorophenyl)lithium **30** was prepared by addition of 1.6 M *n*-butyllithium (7 mL) in hexanes to 1,3-dibromo-5-fluorobenzene (1.5 mL, 11.57 mmol) in anhydrous diethyl ether (2.5 mL) at –78 °C. After stirring for 1 h at the same temperature, the reaction mixture was slowly cannulated into a flask containing a solution of 5-bromovaleronitrile (1 mL, 8.57

mmol) in anhydrous THF (12 mL) and stirred at room temperature for 12 h. After the usual work-up, the crude residue was purified by silica gel column chromatography (dichloromethane/methanol 97:3) to provide **14** as a yellow oil (352 mg, 16% yield). R_f = 0.30 (dichloromethane/methanol 99:1). ^{1}H NMR: δ 1.61–1.69 (m, 2H), 1.78–1.86 (m, 2H), 2.50–2.56 (m, 2H), 3.80–3.85 (m, 2H), 7.21–7.25 (m, 1H), 7.38–7.25 (m, 1H), 7.68–7.71 (m, 1H). ^{13}C NMR: δ 19.7, 21.9, 27.2, 50.2, 112.2 (d, J = 22.4 Hz), 120.0 (d, J = 24.5 Hz), 122.7 (d, J = 9.4 Hz), 125.3 (d, J = 2.9 Hz), 143.8 (d, J = 7.1 Hz), 162.8 (d, J = 248.8 Hz), 163.5. MS (ESI) *m/z* $[M+H]^+$ Calcd for $C_{11}H_{12}BrFN^+$: 256.01. Found: 256.1.

*6.1.3.6. Methyl 3-fluoro-5-(3,4,5,6-tetrahydropyridin-2-yl)benzoate (**31**)*

This compound was prepared according to the method described for compound **25** by employing **14** (200 mg, 0.78 mmol) and MeOH (316 μL) to afford **31** as a yellow oil (57 mg, 31% yield) in 2 h. R_f = 0.38 (cyclohexane/ethyl acetate 7:3). ^{1}H NMR: δ 1.56–1.72 (m, 2H), 1.80–1.89 (m, 2H), 2.57–2.65 (m, 2H), 3.82–3.87 (m, 2H), 3.93 (s, 3H), 7.71–7.76 (m, 2H), 8.18 (s, 1H). ^{13}C NMR: δ 19.6, 22.4, 26.3, 50.1, 53.5, 125.8 (d, J = 22.5 Hz), 126.1 (d, J = 24.7 Hz), 127.4 (d, J = 9.9 Hz), 131.8 (d, J = 2.7 Hz), 141.8 (d, J = 7.2 Hz), 162.7 (d, J = 246.3 Hz), 165.2, 166.3. MS (ESI) *m/z* $[M+H]^+$ Calcd for $C_{13}H_{15}FNO_2^+$: 236.11. Found: 236.2.

*6.1.3.7. (3-Fluoro-5-(3,4,5,6-tetrahydropyridin-2-yl)phenyl)methanol (**15**)*

This compound was prepared according to the method described for compound **6** by employing compound **31** (57 mg, 0.24 mmol) and Red-Al 65% in toluene (308 μL, 1.01 mmol) to afford **15** as a yellow oil (17 mg, 34% yield) in 12h. R_f = 0.20 (cyclohexane/ethyl acetate 2:8). ^{1}H NMR: δ 1.64–1.72 (m, 2H), 1.80–1.88 (m, 2H), 1.92 (br s, 1H), 2.57–2.62 (m,

2H), 3.81–3.85 (m, 2H), 4.69 (s, 2H), 7.06–7.14 (m, 1H), 7.31–7.37 (m, 1H), 7.51–7.53 (m, 1H). ^{13}C NMR: δ 19.8, 21.9, 27.4, 50.0, 64.7, 112.3 (d, J = 22.5 Hz), 114.9 (d, J = 21.7 Hz), 120.0, 142.5 (d, J = 7.4 Hz), 143.7 (d, J = 7.1 Hz), 163.3 (d, J = 244.5 Hz), 165.4. MS (ESI) *m/z* $[M+H]^+$ Calcd for $C_{12}H_{15}FNO^+$: 208.11. Found: 208.2.

6.1.4. Preparation of hydrochlorides of derivatives ***5-15***

*6.1.4.1. 3-(3,4,5,6-Tetrahydropyridin-2-yl)phenol hydrochloride (****5*** **×** ***HCl)***

A solution of the free base **5** (140 mg, 0.80 mmol) in dioxane (1 mL) was treated with a 4.0 M solution of HCl in dioxane. After stirring at room temperature for 30 min, the solvent was removed in vacuo to provide the corresponding salt, which was crystallized from 2-propanol (135 mg, 80%).

5 × HCl: Light brown solid, mp 192–193 °C. ^{1}H NMR (CD_3OD): δ 1.99–2.03 (m, 4H), 3.26–3.29 (m, 2H), 3.82 (m, 2H), 7.18 (dd, J = 8.0, 2.2 Hz, 1H), 7.26 (t, J = 2.2 Hz, 1H), 7.33 (dd, J = 8.0, 1.1 Hz, 1H), 7.45 (dt, J = 8.0, 1.1 Hz, 1H). ^{13}C NMR (CD_3OD): δ 17.0, 17.1, 19.2, 45.2, 114.2, 118.6, 121.9, 130.6, 133.1, 158.6, 183.8. MS (ESI) *m/z* $[M]^+$ Calcd for $C_{11}H_{14}NO^+$: 176.11. Found: 176.4. Anal. Calcd for $C_{11}H_{14}ClNO$ (211.69): C, 62.41; H, 6.67; N, 6.62. Found: C, 62.31; H, 6.89; N, 6.38.

*6.1.4.2. (3-(3,4,5,6-Tetrahydropyridin-2-yl)phenyl)methanol hydrochloride (****6*** **×** ***HCl)***

Crystallized from 2-propanol as light yellow prisms (yield 65%), mp 141–142 °C. ^{1}H NMR (CD_3OD): δ 2.03–2.04 (m, 4H), 3.30–3.32 (m, 2H), 3.84 (m, 2H), 4.72 (s, 2H), 7.62 (t, J = 7.7 Hz, 1H), 7.75–7.80 (m, 2H), 7.87 (m, 1H). ^{13}C NMR: δ 17.0, 17.1, 19.1, 45.3, 62.9, 125.8, 126.5, 129.5, 132.0, 133.2, 143.9, 184.0. MS (ESI) *m/z* $[M+H]^+$ Calcd for $C_{12}H_{16}NO^+$:

190.12. Found: 190.2. Anal. Calcd for $C_{12}H_{16}ClNO$ (225.71): C, 63.85; H, 7.14; N, 6.21. Found: C, 63.75; H, 7.41; N, 6.03.

*6.1.4.3. 6-m-Tolyl-2,3,4,5-tetrahydropyridine hydrochloride (**7** × **HCl**)*

Hygroscopic light brown solid, yield 88%. ^{1}H NMR (CD_3OD): δ 2.01–2.05 (m, 4H), 2.47 (s, 3H), 3.30–3.34 (m, 2H), 3.83–3.87 (m, 2H), 7.50–7.55 (m, 1H), 7.59–7.62 (m, 1H), 7.70–7.75 (m, 2H). ^{13}C NMR (CD_3OD): δ 17.2, 17.3, 19.2, 20.2, 45.3, 125.1, 128.3, 129.4, 132.0, 135.7, 139.9, 183.9. MS (ESI) *m/z* $[M+H]^+$ Calcd for $C_{12}H_{16}N^+$: 174.13. Found: 174.2. Anal. Calcd for $C_{12}H_{16}ClN$ (209.72): C, 68.73; H, 7.69; N, 6.68. Found: C, 68.41; H, 8.02; N, 6.40.

*6.1.4.4. 6-Phenyl-2,3,4,5-tetrahydropyridine hydrochloride (**8** × **HCl**)*

Crystallized from ethanol/diethyl ether (4:1) as a beige solid (yield 91%), mp 88–90 °C. ^{1}H NMR (CD_3OD): δ 2.03 (m, 4H), 3.31 (m, 2H), 3.85 (m, 2H), 7.61–7.66 (m, 2H), 7.74–7.79 (m, 1H), 7.89–7.92 (m, 2H). ^{13}C NMR (CD_3OD): δ 17.2, 17.3, 19.3, 45.5, 128.0 (2C), 129.6 (2C), 132.0, 135.0, 183.8. MS (ESI) *m/z* $[M+H]^+$ Calcd for $C_{11}H_{14}N^+$: 160.11. Found: 160.2. Anal. Calcd for $C_{11}H_{14}ClN$ (195.69): C, 67.51; H, 7.21; N, 7.16. Found: C, 67.41; H, 7.43; N, 7.01.

*6.1.4.5. 6-(3-Fluorophenyl)-2,3,4,5-tetrahydropyridine hydrochloride (**9** × **HCl**)*

Crystallized from 2-propanol as a light brown solid (yield 86%), mp 155 °C dec. ^{1}H NMR (CD_3OD): δ 2.04 (m, 4H), 3.31 (m, 2H), 3.87 (m, 2H), 7.52–7.57 (m, 1H), 7.68–7.76 (m, 3H). ^{13}C NMR (CD_3OD): δ 17.0 (2C), 19.1, 45.7, 115.0 (d, J = 24.5 Hz), 121.6 (d, J = 21.4 Hz), 124.2 (d, J = 2.9 Hz), 131.8 (d, J = 8.0 Hz), 134.0 (d, J = 7.7 Hz), 163.0 (d, J = 246.5 Hz),

183.1. MS (ESI) *m/z* $[M+H]^+$ Calcd for $C_{11}H_{13}FN^+$: 178.10. Found: 178.3. Anal. Calcd for $C_{11}H_{13}ClFN$ (213.68): C, 61.83; H, 6.13; N, 6.56. Found: C, 61.64; H, 6.27; N, 6.31.

*6.1.4.6. 6-(3-Chlorophenyl)-2,3,4,5-tetrahydropyridine hydrochloride (**10** × **HCl**)*

Crystallized from 2-propanol as a beige solid (yield 85%), mp 144 °C dec. ^{1}H NMR (CD_3OD): δ 2.01–2.05 (m, 4H), 3.29–3.32 (m, 2H), 3.86 (m, 2H), 7.62–7.67 (m, 1H), 7.78–7.85 (m, 2H), 7.95–7.97 (m, 1H). ^{13}C NMR (CD_3OD): δ 17.2 (2C), 19.0, 45.5, 126.6, 127.9, 131.1, 133.9, 134.5, 135.4, 183.0. MS (ESI) *m/z* $[M]^+$ Calcd for $C_{11}H_{13}ClN^+$: 194.07. Found: 194.1. Anal. Calcd for (230.13): C, 57.41; H, 5.69; N, 6.09. Found: C, 57.16; H, 5.97; N, 5.88.

*6.1.4.7. 6-(3-Bromophenyl)-2,3,4,5-tetrahydropyridine hydrochloride (**11** × **HCl**)*

Crystallized from 2-propanol/diethyl ether (7:3) as a dark yellow solid (yield 78%), mp 161–164 °C. ^{1}H NMR (CD_3OD): δ 1.99–2.04 (m, 4H), 3.29–3.32 (m, 2H), 3.84 (m, 2H), 7.57 (t, J = 7.9 Hz, 1H), 7.83–7.86 (m, 1H), 7.93–7.97 (m, 1H), 8.07–8.08 (m, 1H). ^{13}C NMR (CD_3OD): δ 16.9 (2C), 19.0, 45.5, 123.2, 126.8, 130.7, 131.2, 134.1, 137.5, 183.1. MS (ESI) *m/z* $[M+H]^+$ Calcd for $C_{11}H_{13}BrN^+$: 238.02. Found: 238.1. Anal. Calcd for $C_{11}H_{13}BrClN$ (274.59): C, 48.12; H, 4.77; N, 5.10. Found: C, 47.85; H, 5.12; N, 4.84.

*6.1.4.8. 6-(3-Iodophenyl)-2,3,4,5-tetrahydropyridine hydrochloride (**12** × **HCl**)*

Crystallized from 2-propanol as a colorless solid (yield 83%), mp 202–204 °C dec. ^{1}H NMR (CD_3OD): δ 2.00–2.04 (m, 4H), 3.27–3.32 (m, 2H), 3.85 (m, 2H), 7.41 (t, J = 7.9 Hz, 1H), 7.88–7.91 (m, 1H), 8.10–8.14 (m, 1H), 8.25 (t, J = 1.8 Hz, 1H). ^{13}C NMR (CD_3OD): δ 16.9, 17.0, 19.0, 45.4, 94.3, 127.3, 131.0, 133.9, 136.5, 143.5, 183.0. MS (ESI) m/z $[M]^+$

Calcd for $C_{11}H_{13}IN^+$: 286.01. Found: 286.0. Anal. Calcd for $C_{11}H_{13}ClIN$ (321.59): C, 41.08; H, 4.07; N, 4.36. Found: C, 40.99; H, 4.32; N, 4.28.

*6.1.4.9. 6-(3,5-Dibromophenyl)-2,3,4,5-tetrahydropyridine hydrochloride (**13** × **HCl**)*

Crystallized from diethyl ether as a colorless solid (yield 44%), mp 95–97 °C. ^{1}H NMR (CD_3OD): δ 2.00–2.03 (m, 4H), 3.26 (m, 2H), 3.86 (m, 2H), 8.07 (d, J = 1.5 Hz, 2H), 8.17 (t, J = 1.5 Hz, 1H). ^{13}C NMR (CD_3OD): δ 16.8 (2C), 18.9, 45.6, 123.8 (2C), 129.8 (2C), 135.5, 139.4, 182.3. MS (ESI) *m/z* $[M]^+$ Calcd for $C_{11}H_{12}Br_2N^+$: 315.93. Found: 316.0. Anal. Calcd for $C_{11}H_{12}Br_2ClN$ (353.48): C, 37.38; H, 3.42; N, 3.96. Found: C, 37.21; H, 3.72; N, 3.88.

*6.1.4.10. 6-(3-Bromo-5-fluorophenyl)-2,3,4,5-tetrahydropyridine hydrochloride (**14** × **HCl**)*

Crystallized from 2-propanol/diethyl ether (7:3) as a dark yellow solid (yield 51%), mp 65 °C dec. ^{1}H NMR (CD_3OD): δ 2.03 (m, 4H), 3.27 (m, 2H), 3.86 (m, 2H), 7.70 (d, J = 8.0 Hz, 1H), 7.82 (d, J = 8.0 Hz, 1H), 7.92 (s, 1H). ^{13}C NMR (CD_3OD): δ 16.9 (2C), 18.9, 45.7, 114.4 (d, J = 24.5 Hz), 123.8 (d, J = 9.7 Hz), 124.7 (d, J = 24.5 Hz), 127.1 (d, J = 3.1 Hz), 135.4 (d, J = 8.6 Hz), 162.8 (d, J = 251.1 Hz), 182.7. MS (ESI) *m/z* $[M]^+$ Calcd for $C_{11}H_{12}BrFN^+$: 256.01. Found: 256.0. Anal. Calcd for $C_{11}H_{12}BrClFN$ (292.58): C, 45.16; H, 4.13; N, 4.79. Found: C, 44.91; H, 4.39; N, 4.52.

*6.1.4.11. (3-Fluoro-5-(3,4,5,6-tetrahydropyridin-2-yl)phenyl)methanol hydrochloride (**15** × **HCl**)*

Hygroscopic dark yellow solid, yield 75%. ^{1}H NMR (CD_3OD): δ 2.01–2.05 (m, 4H), 3.30–3.32 (m, 2H), 3.84–3.86 (m, 2H), 4.72 (s, 2H), 7.52–7.58 (m, 2H), 7.69 (m, 1H). ^{13}C NMR: δ 17.1 (2C), 19.1, 45.3, 62.8, 115.3 (d, J = 18.3 Hz), 125.2 (d, J = 2.9 Hz), 132.7 (d, J

= 7.4 Hz), 133.2 (d, *J* = 24.2 Hz), 143.8 (d, *J* = 7.1 Hz), 163.0 (d, *J* = 247.9 Hz), 183.8. MS (ESI) *m/z* $[M+H]^+$ Calcd for $C_{12}H_{15}FNO^+$: 208.11. Found: 208.2. Anal. Calcd for $C_{12}H_{15}ClFNO$ (243.71): C, 59.14; H, 6.20; N, 5.75. Found: C, 58.79; H, 6.54; N, 5.43.

6.2. Pharmacology

6.2.1. Receptor binding assays

Details of the binding experiments to the nicotinic receptor subtypes have been recently reported for the α4β2 and α7 subtypes [57] as well as for the α3β4 subtype [58]. The K_i values of the novel compounds **5-15** were determined by pre-incubating cortex or hippocampus homogenates with increasing doses (10 pM - 10 mM) of the reference nicotinic agonists, epibatidine or nicotine, and the drug to be tested for 30 min at room temperature, followed by overnight incubation with a final concentration of 0.100 nM [^{3}H]-epibatidine (cortex) or 1 nM [^{125}I]-α-bungarotoxin (hippocampus), at the same temperatures as those used for the saturation experiments.

In the case of HEK 293 transfected α3β4 receptors, the inhibition of [^{3}H]epibatidine binding by the studied derivatives was measured by incubating increasing concentrations of the compounds for 5 min followed by overnight incubation with 0.25 nM [^{3}H]epibatidine. For each subtype, the experimental data were analyzed using the LIGAND program as described by Munson and Rodbard [59]. The binding parameters were calculated by simultaneously fitting three independent saturation experiments and the K_i values were determined by fitting the data of three independent competition experiments. The errors in the K_D and K_i values of the simultaneous fits were calculated using the LIGAND software, and were expressed as percentage coefficients of variation (% CV). When final compound concentrations up to 100

μM did not inhibit radioligand binding, the K_i value was defined as being > 100 μM based on the Cheng and Prusoff's equation [60].

6.2.2. Electrophysiological recordings

The human α7, α4β2 and α3β4 nAChRs were expressed by transient transfection in the rat anterior pituitary GH4C1 cell line [61], grown in Ham's F10 medium supplemented with 10% heat-inactivated FBS and 1% penicillin/streptomycin, at 37°C in a 5% CO_2 humidified atmosphere. Cells were plated on poly-L-lysine-coated coverslides (1×10^5 cells/mL) and transiently transfected 24 h later using Magnetofection™: NeuroMag (OZ Biosciences, France) according to manufacturer's protocol, adding 0.5 μg of each cDNA subtype per well. All culture media were purchased from Invitrogen (San Giuliano Milanese, Italy). Whole-cell current recordings were performed 2-3 days after plating. Recordings and data analysis were performed by using borosilicate glass patch pipette (3- to 6-MΩ tip resistance) connected to an Axopatch 200A amplifier (Axon Instruments, Foster City, CA). Data were stored on a PC computer by using PCLAMP10 software (Molecular Devices). During the recording period, the cells were bathed in the following solution (mM): 140 NaCl, 2 $CaCl_2$, 2.8 KCl, 2 $MgCl_2$, 10 Hepes/NaOH and 10 glucose; pH 7.3. The patch pipettes were filled with a solution containing (mM): 140 CsCl, 2 MgATP, 10 Hepes/CsOH and 5 BAPTA; pH 7.3. Whole-cell capacitance and patch series resistance (3-5 MΩ) were estimated from slow transient compensations. A series resistance compensation of 85-90% was obtained in all cases. The cells were voltage-clamped at a holding potential of −70 mV and continuously perfused with a gravity-driven system using independent external tubes for the control and agonist-containing solutions. These tubes were positioned 50-100 μm from the patched cell and

connected to a fast exchanger system (RSC-160, BioLogic, France). Dose-response relationships were constructed by sequentially applying different concentrations of agonists, and normalizing the obtained current amplitudes to the value obtained by applying 1 mM ACh on the same cell. For quantitative estimations of agonist actions, dose-response relationship were fitted to the Equation (1):

$$I = I_{max} \{[C]^{nH} / (EC_{50}^{nH} + [C]^{nH})\} \quad (1)$$

where I is the current amplitude induced by the agonist at concentration [*C*], I_{max} is the maximum response of the cell, nH is the Hill coefficient and EC_{50} is the concentration for which a half maximum response is induced.

6.3. Docking and MD simulations

The α4β2, α3β4 and α7 nAChR models [62,63,37], obtained by homology modeling on the crystal structure of *A*-AChBP/**1** (PDB accession code 2BYQ), were utilized to design and to rationalize the results obtained for the compounds under investigation. The receptor models were previously geometrically refined following the molecular modeling standard procedures: minimization, equilibration and molecular dynamics simulation. Ligands utilized for docking were preliminarily minimized by Gaussian09 [64] at the DFT/B3LYP/6-31G(d) level. The net charge of all ligands was +1. Docking calculations were then performed with the GOLD 5.2 program [65] into the binding cleft depicted by α4-Trp147 and the homologue residues in the α3 and α7 subtypes. The cavity was detected with an active site radius of 12.0 Å from the carbonyl oxygen atom of the Trp residue. The PLP fitness function was used to assign the score to the different docking poses and the genetic algorithm parameters were kept at the default value. Cluster analysis was performed by means of the GOLD internal algorithm, based on the RMSD of each pose compared with the one previously obtained. The solutions

with the highest score, belonging to the first cluster, were visually inspected and then chosen for further analysis. Then, the resulting complexes were submitted to molecular dynamics (MD) simulations with the *sander* and *pmemd.cuda* modules of the AMBER12 [66] package. *ff12* [64] and *GAFF* [67] force fields were applied for the protein and the ligands, respectively. The complexes were immersed in a box containing about 30000 water molecules and the TIP3P model was employed to explicitly represent the solvent [68]. Counter ions were added to neutralize the total charge of the simulating systems.

At first, the energy of the water molecules was minimized, keeping the atoms of the protein frozen. Then, a minimization of the whole system was performed by setting a convergence criterion on the gradient of 10^{-4} kcal mol^{-1} $Å^{-1}$. Prior to starting the MD simulations, the system was equilibrated for 40 ps at 300 K in isocore conditions (NVT). Subsequently, 50 ns of MD simulations in isothermal-isobaric ensemble were carried out at 300 K with a 2 fs time-step (NPT). In the production runs, the systems were performed in periodic boundary conditions. Van der Waals and short-range electrostatic interactions were estimated within a 8 Å cutoff. SHAKE algorithm was applied to all bonds involving hydrogen atoms. When the geometrical stabilization of the complexes was reached, a new minimization of the whole system was performed. The water occupancy over a 50 ns MD simulations was calculated by VolMap tool of VMD [38]. Figures were acquired by the PyMOL software (The PyMOL Molecular Graphics System).

Acknowledgments

This research was financially supported by the Italian Ministry of Education, University and Research (PRIN grant 2009-R7WCZS to C. G., S. F., and M. D. A.), and by the CNR

Research Project on Aging, the Regione Lombardia Projects MbMM-convenzione n°18099/RCC (C. G.). F. F. is recipient of a fellowship from Fondazione Vollaro. We acknowledge CINECA and the Regione Lombardia award under the LISA initiative for high-performance computing resources and financial support.

References

[1] C. Gotti, M. Zoli, F. Clementi, Brain nicotinic acetylcholine receptors: native subtypes and their relevance, Trends Pharmacol. Sci. 27 (2006) 482-491.

[2] J.A. Dani, D. Bertrand, Nicotinic acetylcholine receptors and nicotinic cholinergic mechanisms of the central nervous system, Ann. Rev. Pharmacol. Toxicol. 47 (2007) 699-729.

[3] R. Hurst, H. Rollema, D. Bertrand, Nicotinic acetylcholine receptors: from basic science to therapeutics, Pharmacol. Therapeut. 137 (2013) 22-54.

[4] M. Zoli, C. Léna, M.R. Picciotto, J.P. Changeux, Identification of four classes of brain nicotinic receptors using beta2 mutant mice, J. Neurosci. 18 (1998) 4461-4472.

[5] P. Seguela, J. Wadiche, K. Dineley-Miller, J.A. Dani, J.W. Patrick, Molecular cloning, functional properties, and distribution of rat brain α_7: a nicotinic cation channel highly permeable to calcium, J. Neurosci. 13 (1993) 596-604.

[6] C.M. Flores, R.M. DeCamp, S. Kilo, S.W. Rogers, K.M. Hargreaves, Neuronal nicotinic receptor expression in sensory neurons of the rat trigeminal ganglion: demonstration of alpha3beta4, a novel subtype in the mammalian nervous system, J. Neurosci. 16 (1996) 7892-7901.

[7] M.W. Quick, R.M. Cebalios, M. Kasten, J.M. McIntosh, R.A. Lester, Alpha3-beta4 subunit-containing nicotinic receptors dominate function in rat medial habenula neurons, Neuropharmacology 38 (1999) 769-783.

[8] S.R. Grady, M. Moretti, M. Zoli, M.J. Marks, A. Zanardi, L. Pucci, F. Clementi, C. Gotti, Rodent habenulo-interpeduncular pathway expresses a large variety of uncommon nAChR subtypes, but only the alpha3beta4* and alpha3beta3beta4*

subtypes mediate acetylcholine release, J. Neurosci. 29 (2009) 2272-2282.

[9] M.R. Picciotto, M. Zoli, C. Léna, A. Bessis, Y. Lallemand, N. Le Novere, P. Vincent, E.M. Pich, P. Brulet, J.P. Changeux, Abnormal avoidance learning in mice lacking functional high affinity nicotine receptor in the brain, Nature 374 (1995) 65-67.

[10] E.D. Levin, A. Bradley, N. Addy, N. Sigurani, Hippocampal alpha7 and alpha4beta2 nicotinic receptors and working memory, Neuroscience 109 (2002) 757-765.

[11] L.M. Marubio, M. del Mar Arroyo-Jimenez, M. Cordero-Erausquin, C. Léna, N. Le Novere, A. de Kerchove d'Exaerde, M. Huchet, M.I. Damaj, J.P. Changeux, Reduced antinociception in mice lacking neuronal nicotinic receptor subunits, Nature 398 (1999) 805-810.

[12] L. Di Cesare Mannelli, A. Pacini, C. Matera, M. Zanardelli, T. Mello, M. De Amici, C. Dallanoce, C. Ghelardini, Involvement of α7 nAChR subtype in rat oxaliplatin-induced neuropathy: Effects of selective activation, Neuropharmacology 79 (2014) 37-48.

[13] M.R. Picciotto, M. Zoli, Neuroprotection via nAChRs: the role of nAChRs in neurodegenerative disorders such as Alzheimer's and Parkinson's disease, Front Biosci. 13 (2008) 492-504.

[14] S. Llabrés, S. García-Ratés, E. Cristóbal-Lecina, A. Riera, J.I. Borrell, J. Camarasa, D. Pubill, F.J. Luque, E. Escubedo, Molecular basis of the selective binding of MDMA enantiomers to the alpha4beta2 nicotinic receptor subtype: synthesis, pharmacological evaluation and mechanistic studies, Eur. J. Med. Chem. 81 (2014) 35-46.

[15] A. Nencini, C. Castaldo, T.A. Comery, J. Dunlop, E. Genesio, C. Ghiron, S. Haydar, L. Maccari, I. Micco, E. Turlizzi, R. Zanaletti, J. Zhang, Design and synthesis of a hybrid series of potent and selective agonists of α7 nicotinic acetylcholine receptor, Eur. J. Med. Chem. 78 (2014) 401-418.

[16] M. De Biasi, Nicotinic mechanism in the autonomic control of organ systems, J. Neurobiol. 53 (2002) 568-579.

[17] B. Antolin-Fontes, J.L. Ables, A. Gorlich, I. Ibanez-Tallon, The habenulo-interpeduncular pathway in nicotine aversion and withdrawal, Neuropharmacology 96 (2015) 213-222.

[18] K.J. Jackson, P.P. Muldoon, M. De Biasi, M.I. Damaj, New mechanisms and perspectives in nicotine withdrawal, Neuropharmacology 96 (2015) 223-234.

[19] S.D. Glick, E.M. Sell, S.E. McCallum, I.M. Maisonneuve, Brain regions mediating alpha3beta4 nicotinic antagonist effects of 18-MC on nicotine self-administration, Eur. J. Pharmacol. 669 (2011) 71-75.

[20] S.D. Glick, E.M. Sell, I.M. Maisonneuve, Brain regions mediating alpha3beta4 nicotinic antagonist effects of 18-MC on methamphetamine and sucrose self-administration, Eur. J. Pharmacol. 599 (2008) 91-95.

[21] M.R. Improgo, M.D. Scofield, A.R. Tapper, P.D. Gardner, The nicotinic acetylcholine receptor CHRNA5/A3/B4 gene cluster: dual role in nicotine addiction and lung cancer, Prog. Neurobiol. 92 (2010) 212-226.

[22] M.R. Improgo, L.G. Soll, A.R. Tapper, P.D. Gardner, Nicotinic acetylcholine receptors mediate lung cancer growth, Front. Physiol. 4 (2013) 251.

[23] K. Brejc, W.J. van Dijk, R.V. Klaassen, M. Schuurmans, J. van Der Oost, A.B. Smit, T.K. Sixma, Crystal structure of an ACh-binding protein reveals the ligand-binding domain of nicotinic receptors, Nature 411 (2001) 269-276.

[24] P.H. Celie, S.E. van Rossum-Fikkert, W.J. van Dijk, K. Brejc, A.B. Smit, T.K. Sixma, Nicotine and carbamylcholine binding to nicotinic acetylcholine receptors as studied in AChBP crystal structures, Neuron 41 (2004) 907-914.

[25] S.B. Hansen, G. Sulzenbacher, T. Huxford, P. Marchot, P. Taylor, Y. Bourne, Structures of *Aplysia* AChBP complexes with nicotinic agonists and antagonists reveal distinctive binding interfaces and conformations, EMBO J. 24 (2005) 3635-3646.

[26] S.B. Hansen, T.T. Talley, Z. Radic, P. Taylor, Structural and ligand recognition characteristics of an acetylcholine-binding protein from *Aplysia californica*, J. Biol. Chem. 279 (2004) 24197-24202.

[27] P. Rucktooa, C.A. Haseler, R. van Elk, A.B. Smit, T. Gallagher, T.K. Sixma, Structural characterization of binding mode of smoking cessation drugs to nicotine acetylcholine receptors through study of ligand complexes with acetylcholine binding protein, J. Biol. Chem. 287 (2012) 23283-23293.

[28] A.P. Blum, E.B. Van Arnam, L.A. German, H.A. Lester, D.A. Dougherty, Binding interactions to the complementary subunit of nicotinic receptors, J. Biol. Chem.

288 (2013) 6991-6997.

[29] S. Amiri, M.S.P. Sansom, P.C. Biggin, Molecular dynamics studies of AChBP with nicotine and carbamylcholine: the role of water in the binding pocket, Protein Eng. Des. Sel. 20 (2007) 353-359.

[30] A.P. Blum, H.A. Lester, D.A. Dougherty, Nicotinic pharmacophore: the pyridine N of nicotine and carbonyl of acetylcholine hydrogen bond across a subunit interface to a backbone NH, Proc. Natl. Acad. Sci. USA 107 (2010) 13206-13211.

[31] C. Dallanoce, G. Grazioso, D.Y. Pomè, M. Sciaccaluga, C. Matera, C. Gotti, S. Fucile, M. De Amici, Investigating the hydrogen-bond acceptor site of the nicotinic pharmacophore model: a computational and experimental study using epibatidine-related molecular probes, J. Comput. Aid. Mol. Des. 27 (2013) 975-987.

[32] W.R. Kem, V.M. Mahnir, R.L. Papke, C.J. Lingle, Anabaseine is a potent agonist on muscle and neuronal *alpha*-Bungarotoxin-sensitive nicotinic receptors, J. Pharmacol. Exp. Ther. 283 (1997) 979-992.

[33] R.L. Papke, E.M. Meyer, S. Lavieri, S.R. Bollampally, T.A.S. Papke, N.A. Horenstein, Y. Itoh, J.K. Porter Papke, Effects at a distance in α7 nAChR selective agonists: benzylidene substitutions that regulate potency and efficacy, Neuropharmacology 46 (2004) 1023-1038.

[34] J.D.R. Knight, D. Hamelberg, J.A. McCammon, R. Kothary, The role of conserved water molecules in the catalytic domain of protein kinases, Proteins: Structure, Function, and Bioinformatics 76 (2009) 527-535.

[35] S.B.A. de Beer, N.P.E. Vermeulen, C. Oostenbrink, The role of water molecules in computational drug design, Curr. Top. Med. Chem. 10 (2010) 55-66.

[36] A. Kumar, K.Y.J. Zhang, Investigation on the effect of key water molecules on docking performance in CSARdock exercise, J. Chem. Inf. Model. 53 (2013) 1880-1892.

[37] F. Mazzo, F. Pistillo, G. Grazioso, F. Clementi, N. Borgese, C. Gotti, Nicotine-modulated subunit stoichiometry affects stability and trafficking of α3β4 nicotinic receptor, J. Neurosci. 33 (2013) 12316-12328.

[38] For occupancy definition see http://www.ks.uiuc.edu/Research/vmd/plugins/volmapgui.

[39] E. Specker, J. Böttcher, S. Brass, A. Heine, H. Lilie, A. Schoop, G. Müller, N.

Griebenow, G. Klebe, Unexpected novel binding mode of pyrrolidine-based aspartyl protease inhibitors: design, synthesis and crystal structure in complex with HIV protease, ChemMedChem 1 (2006) 106-117.

[40] M.Z. Hernandes, S.M.T. Cavalcanti, D.R.M. Moreira, W.F. De Azevedo Jr, A.C.L. Leite, Halogen atoms in the modern medicinal chemistry: hints for the drug design, Curr. Drug Targets 11 (2010) 303-314.

[41] Y.X. Lu, J.W. Zou, J.C. Fan, W.N. Zhao, Y.J. Jiang, Q.S. Yu, *Ab initio* calculations on halogen-bonded complexes and comparison with density functional methods, J. Comput. Chem. 30 (2009) 725-732.

[42] A. Giovannini, D. Savoia, A. Umani-Ronchi, Organometallic ring-opening reactions of *N*-acyl and *N*-alkoxycarbonyl lactams. Synthesis of cyclic imines, J. Org. Chem. 54 (1989) 228-234.

[43] D.R. Dragoli, M.T. Burdett, J.A. Ellman, Design, synthesis, and utility of a support-bound *tert*-Butanesulfinamide, J. Amer. Chem. Soc. 123 (2001) 10127-10128.

[44] J. Georgsson, A. Hallberg, M. Larhed, Rapid palladium-catalyzed synthesis of esters from aryl halides utilizing $Mo(CO)_6$ as a solid carbon monoxide source, J. Comb. Chem. 5 (2003) 350-352.

[45] Y. Wada, N. Nishida, N. Kurono, T. Ohkuma, K. Orito, Synthesis of a 3-arylisoquinoline alkaloid, decumbenine B, Eur. J. Org. Chem. 26 (2007) 4320-4327.

[46] D.F. Fry, C.B. Fowler, R.K. Dieter, Synthesis of cyclic imines by addition of Grignard reagents to ω-bromonitriles, Synlett 10 (1994) 836-838.

[47] V. Gallulo, L. Dimas, C.A. Zezza, M.B. Smith, Cyclization of ω-halonitriles with organolithiums, Org. Prep. Proced. Int. 21 (1989) 297-301.

[48] T.J. Sisto, M.R. Golder, E.S. Hirst, R. Jasti, Selective synthesis of strained [7]cycloparaphenylene: an orange-emitting fluorophore, J. Amer. Chem. Soc. 133 (2011) 15800-15802.

[49] D. Colquhoun, Binding, gating, affinity and efficacy: the interpretation of structure-activity relationships for agonists and of the effects of mutating receptors, Brit. J. Pharmacol. 125 (1998) 924-947.

[50] L.A. Rohde, P.K. Ahring, M.L. Jensen, E.O. Nielsen, D. Peters, C. Helgstrand, C.

Krintel, K. Harpsoe, M. Gajhede, J.S. Kastrup, T. Balle, Intersubunit bridge formation governs agonist efficacy at nicotinic acetylcholine α4β2 receptors: unique role of halogen bonding revealed, J. Biol. Chem. 287 (2012) 4248-4259.

[51] N. Mukhtasimova, S.M. Sine, Nicotinic receptor transduction zone: invariant arginine couples to multiple electron-rich residues, Biophys. J. 104 (2013) 355-367.

[52] S. Frahm, M.A. Slimak, L. Ferrarese, J. Santos-Torres, B. Antolin-Fontes, S. Auer, S. Filkin , S. Pons, J.F. Fontaine, V. Tsetlin, U. Maskos, I. Ibanez-Tallon, Aversion to nicotine is regulated by the balanced activity of beta4 and alpha5 nicotinic receptor subunits in the medial habenula, Neuron 70 (2011) 522-535.

[53] R. Salas, R. Sturm, J. Boulter, M. De Biasi, Nicotinic receptors in the habenulo-interpeduncular system are necessary for nicotine withdrawal in mice, J. Neurosci. 29 (2009) 3014-3018.

[54] I.M. Maisonneuve, S.D. Glick, 2003. Anti-addictive actions of an iboga alkaloid congener: a novel mechanism for a novel treatment, Pharmacol. Biochem. Behav. 75 (2003) 607-618.

[55] L. Toll, N.T. Zaveri, W.E. Polgar, F. Jiang, T.V. Khroyan, W. Zhou, X.(S.) Xie, G.B. Stauber, M.R. Costello, F.M. Leslie, AT-1001: A high affinity and selective α3β4 nicotinic acetylcholine receptor antagonist blocks nicotine self-administration in rats, Neuropsychopharmacol. 37 (2012) 1367-1376.

[56] J.A. Zoltewicz, M.P. Cruskie Jr, A superior synthesis of cholinergic anabaseine, Org. Prep. Proced. Int. 27 (1995) 510-513.

[57] C. Matera, L. Pucci, C. Fiorentini, S. Fucile, C. Missale, G. Grazioso, F. Clementi, M. Zoli, M. De Amici, C. Gotti, C. Dallanoce, Bifunctional compounds targeting both D_2 and non-alpha7 nACh receptors: design, synthesis and pharmacological characterization, Eur. J. Med. Chem. 101 (2015) 367-383.

[58] M. Sala, D. Braida, L.Pucci, I. Manfredi, M.J. Marks, C.R.Wageman, S.R. Grady, B. Loi, S. Fucile, F. Fasoli, M. Zoli, B. Tasso, F. Sparatore, F. Clementi, C. Gotti, CC4, a dimer of cytisine, is a selective partial agonist at alpha4beta2/alpha6beta2 nAChR with improved selectivity for tobacco smoking cessation, Br. J. Pharmacol. 168 (2013) 835-849.

[59] P.J. Munson, D. Rodbard, Ligand: a versatile computerized approach for characterization of ligand-binding systems, Anal. Biochem. 107 (1980) 220-239.

[60] Y. Cheng, W.H. Prusoff, Relationship between the inhibition constant (K1) and the concentration of inhibitor which causes 50 per cent inhibition (I50) of an enzymatic reaction, Biochem. Pharmacol. 22 (1973) 3099-3108.

[61] S. Fucile, M. Renzi, P. Lax, F. Eusebi, Fractional Ca^{2+} current through human neuronal α7 nicotinic acetylcholine receptors, Cell Calcium 34 (2003) 205-209.

[62] G. Grazioso, D.Y. Pomè, C. Matera, F. Frigerio, L. Pucci, C. Gotti, C. Dallanoce, M. De Amici, Design of novel alpha7-subtype-preferring nicotinic acetylcholine receptor agonists: application of docking and MM-PBSA computational approaches, synthetic and pharmacological studies, Bioorg. Med. Chem. Lett. 19 (2009) 6353-6357.

[63] G. Grazioso, A. Cavalli, M. De Amici, M. Recanatini, C. De Micheli, Alpha7 nicotinic acetylcholine receptor agonists: Prediction of their binding affinity through a molecular mechanics Poisson-Boltzmann surface area approach, J. Comp. Chem. 29 (2008) 2593-2602.

[64] Gaussian 09, Revision A.02, M.J. Frisch, G.W. Trucks, H.B. Schlegel, G.E. Scuseria, M.A. Robb, J.R. Cheeseman, G. Scalmani, V. Barone, B. Mennucci, G.A. Petersson, H. Nakatsuji, M. Caricato, X. Li, H.P. Hratchian, A.F. Izmaylov, J. Bloino, G. Zheng, J.L. Sonnenberg, M. Hada, M. Ehara, K. Toyota, R. Fukuda, J. Hasegawa, M. Ishida, T. Nakajima, Y. Honda, O. Kitao, H. Nakai, T. Vreven, J.A. Montgomery Jr, J.E. Peralta, F. Ogliaro, M. Bearpark, J.J. Heyd, E. Brothers, K.N. Kudin, V.N. Staroverov, R. Kobayashi, J. Normand, K. Raghavachari, A. Rendell, J.C. Burant, S.S. Iyengar, J. Tomasi, M. Cossi, N. Rega, M.J. Millam, M. Klene, J.E. Knox, J.B. Cross, V. Bakken, C. Adamo, J. Jaramillo, R. Gomperts, R.E. Stratmann, O. Yazyev, A.J. Austin, R. Cammi, C. Pomelli, J.W. Ochterski, R.L. Martin, K. Morokuma, V.G. Zakrzewski, G.A. Voth, P. Salvador, J.J. Dannenberg, S. Dapprich, A.D. Daniels, Ö. Farkas, J.B. Foresman, J.V. Ortiz, J. Cioslowski, D.J. Fox, Gaussian, Inc., Wallingford CT (2009).

[65] Gold v. 5.2.; Cambridge Crystallographic Data Centre, Cambridge, UK.

[66] D.A. Case, T.A. Darden, T.E. Cheatham III, C.L. Simmerling, J. Wang, R.E. Duke, R. Luo, C. Walker, W. Zhang, K.M. Merz, B. Roberts, S. Hayik, A. Roitberg, G. Seabra, J. Swails, A.W. Goetz, I. Kolossváry, K.F. Wong, F. Paesani, J. Vanicek, R.M. Wolf, J. Liu, X. Wu, S.R. Brozell, T. Steinbrecher, H. Gohlke, Q. Cai, X. Ye, J. Wang, M.J. Hsieh, G. Cui, D.R. Roe, D.H. Mathews, M.G. Seetin, R. Salomon-Ferrer, C. Sagui, V.

Babin, T. Luchko, S. Gusarov, A. Kovalenko, P.A. Kollman, AMBER 12, University of California, San Francisco (2012).

[67] J. Wang, R.M. Wolf, J.W. Caldwell, P.A. Kollman, D.A. Case, Development and testing of a general amber force field, J. Comput. Chem. 25 (2004) 1157-1174.

[68] W.L. Jorgensen, J. Chandrasekhar, J.D. Madura, R.W. Impey, L.M. Klein, Comparison of simple potential functions for simulating liquid water, J. Chem. Phys. 79 (1983) 926-936.

[69] M. Avalos, M.J. Parker, F.N. Maddox, F.I. Carrol, C.W. Luetje, Effects of pyridine ring substitutions on affinity, efficacy, and subtype selectivity of neuronal nicotinic receptor agonist epibatidine, J. Pharm. Exp. Ther. 302 (2002) 1246-1252.

[70] J.P. Sullivan, D. Donnelly-Roberts, C.A. Briggs, D.J. Anderson, M. Gopalakrishnan, M. Piattoni-Kaplan, J.E. Campbell, D.G. McKenna, E. Molinari, A.M. Hettinger, D.S. Garvey, J.T. Wasicak, M.W. Holladay, M. Williams, S.P. Arneric, A-85380 [3-(2(*S*)-azetidinylmethoxy) pyridine]: *in vitro* pharmacological properties of a novel, high affinity α4β2 nicotinic acetylcholine receptor ligand, Neuropharmacology 35 (1996) 725-734.

Captions to Figures and Schemes

Figure 1. Structure of the reference compounds **1-4**[a] and of the new derivatives **5-15**[b] investigated in this study. [a](±)-**3**: R_1 = H, R_2 = OH; (±)-**4**: R_1 = H, R_2 = CH_2OH; [b]**5**: R_1 = H, R_2 = OH; **6**: R_1 = H, R_2 = CH_2OH; **7**: R_1 = H, R_2 = CH_3; **8**: R_1 = R_2 = H; **9**: R_1 = H, R_2 = F; **10**: R_1 = H, R_2 = Cl; **11**: R_1 = H, R_2 = Br; **12**: R_1 = H, R_2 = I; **13**: R_1 = Br, R_2 = Br; **14**: R_1 = F, R_2 = Br; **15**: R_1 = F, R_2 = CH_2OH.

Figure 2. (**A**) Hypothetical binding mode of anabaseine **2** within the α3β4 binding site. In this frame of MD simulation, WAT molecules engaged H-bond interactions with β4-Leu119 and β4-Thr106. In the equilibrated system, water molecules created H-bond network also with the α3-Trp149 side chain. (**B**) Distance fluctuation between the oxygen atom of WAT and the protein residue involved in the H-bond network in the binding site of the α3β4 model in complex with **2**.

Figure 3. Average water occupancy (dark yellow areas) calculated by the VolMap tool of VMD over 50 ns of MD simulations. The surface was plotted considering an isovalue of 0.6.

Figure 4. Dose-current response relationships for derivatives **6**, **12** and **13** administered to GH4C1 cells expressing human α3β4, α4β2 or α7 nAChRs. (**A**) Current amplitudes elicited by compound **6**, and mediated by α3β4 (●; n=7), α4β2 (■; n=5) or α7 (△; n=5) nAChRs, were normalized to the current amplitude elicited on the same cell by ACh 1 mM. Solid lines represent best fit curves (see Experimental Section) yielding the following parameters: EC_{50} values of 20 ± 1 μM and 60 ± 2 μM, nH values of 1.4 ± 0.3 and 3.3 ± 0.4, for α3β4 and α7 nAChRs, respectively. (**B**) Normalized current amplitudes elicited by compound **12**, and mediated by α3β4 (●; n=8), α4β2 (■; n=21) or α7 (△; n=12) nAChRs. Solid line represents the best fit curve for α3β4 nAChR, yielding the following parameters: EC_{50} = 7.4 ± 2.9 μM and nH = 0.97 ± 0.3. (**C**) Normalized current amplitudes elicited by compound **13**, and mediated by α3β4 (●; n=22), α4β2 (■; n=5) or α7 (△; n=5) nAChRs.

Figure 5. Hypothetical binding mode of **12** within the α3β4 nAChR binding site.

Scheme 1. Synthesis of target compounds **5**, **6**, **10**, **12** and **13**. Reagents and conditions: (a) 2.5 M BuLi/hexane (1 equiv), $(Boc)_2O$ (1 equiv), THF, –78°C, 7 h; (b) CF_3COOH (16 equiv), rt, 4 h; (c) 48% HBr, reflux 6 h, then rt, 12 h; (d) $Mo(CO)_6$ (1.5 equiv), 10% Pd/C, DMAP (2 equiv), DIPEA (2 equiv), MeOH (10 equiv), 1,4-dioxane, MW, 50 W, 130°C, 1 h; (e) 65% Red-Al/toluene (4.2 equiv), THF, rt, 1 h; (f) 4N HCl (5 equiv), 1,4-dioxane, rt, 30 min.

Scheme 2. Synthesis of target compounds **7**, **8**, **9**, **11**, **14** and **15**. Reagents and conditions: (a) anhydrous THF, rt, 1-12 h (**27**, 75 °C, 3 h); (b) $Mo(CO)_6$ (3 equiv), 10% Pd/C, DMAP (2 equiv), DIPEA (2 equiv), MeOH (10 equiv), 1,4-dioxane, MW, 50 W, 130°C, 2 h; (c) 65% Red-Al/toluene (8.4 equiv), THF, rt, 12 h; (d) 4N HCl (5 equiv), 1,4-dioxane, rt, 30 min.

Table 1. Binding affinities of reference compounds **1-4** and of new derivatives **5-15** at α3β4, α4β2 and α7 nAChR subtypes.

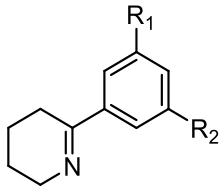

5-15

Compound	R_1	R_2	K_i (nM)[a] α3β4[b]	α4β2[c]	α7[d]	α3β4 vs α4β2 selectivity	α3β4 vs α7 selectivity
Epibatidine (–)-**1**			0.3[e]	0.030[e]	16/22[f]	0.1	53
Anabaseine **2**[g]			107 (33)	67 (15)	32 (43)	0.6	0.3
(±)-**3**	H	OH	80 (26)	127 (11)	609 (36)	1.6	7.6
(±)-**4**	H	CH_2OH	92 (24)	429 (14)	1800 (35)	4.7	20
5	H	OH	680 (23)	32000 (8)	9300 (42)	47	14
6	H	CH_2OH	80 (35)	35000 (13)	158 (35)	438	2.0
7	H	CH_3	155 (20)	1450 (37)	384 (53)	9.4	2.5
8	H	H	194 (35)	2080 (20)	2400 (53)	11	12
9	H	F	108 (20)	2040 (23)	2370 (57)	19	22
10	H	Cl	77.2 (33)	11500 (62)	394 (38)	149	5.1
11	H	Br	29.8 (32)	5020 (45)	43.2 (37)	168	1.5
12	H	I	4.7 (37)	3790 (44)	11.3 (29)	806	2.4
13	Br	Br	70.8 (30)	18800 (41)	343 (47)	266	4.8
14	F	Br	48 (17)	1770 (21)	204 (44)	37	4.3
15	F	CH_2OH	80 (24)	744 (38)	821 (43)	9.3	10

[a]K_i values are derived from three competition-binding experiments. The numbers in brackets refer to the % coefficients of variation. [b]α3β4 nAChRs heterologously expressed in HEK 293 cells. [c]Native α4β2 nAChRs present in rat cortical membranes. [d]Native α7 nAChRs present in rat hippocampal membranes. [e]K_d value from Ref. 69. [f]Binding affinity data for the (–) and (+) enantiomers of **1** are from Ref. 70. [g]The dihydrochloride of **2** was assayed.

Table 1
(Carlo Matera et al.)

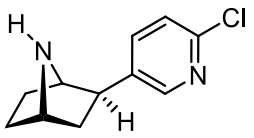

(–)-**1**: Epibatidine

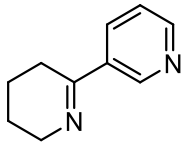

2: Anabaseine

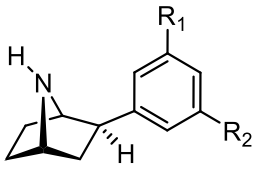

(±)-**3**, (±)-**4**

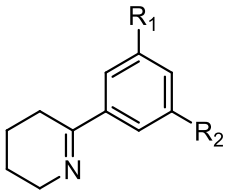

5-15

Figure 1
(Carlo Matera et al.)

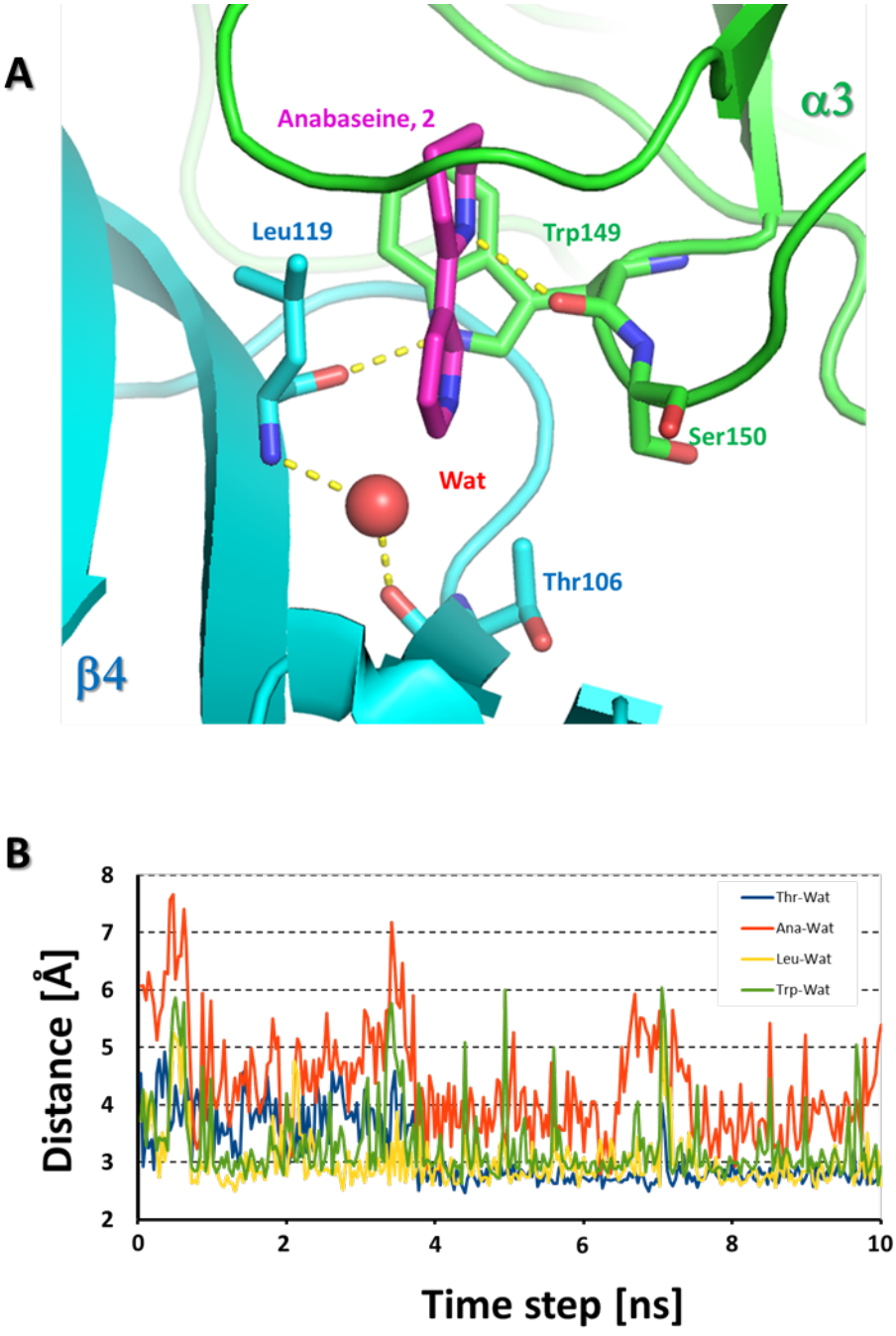

Figure 2
(Carlo Matera et al.)

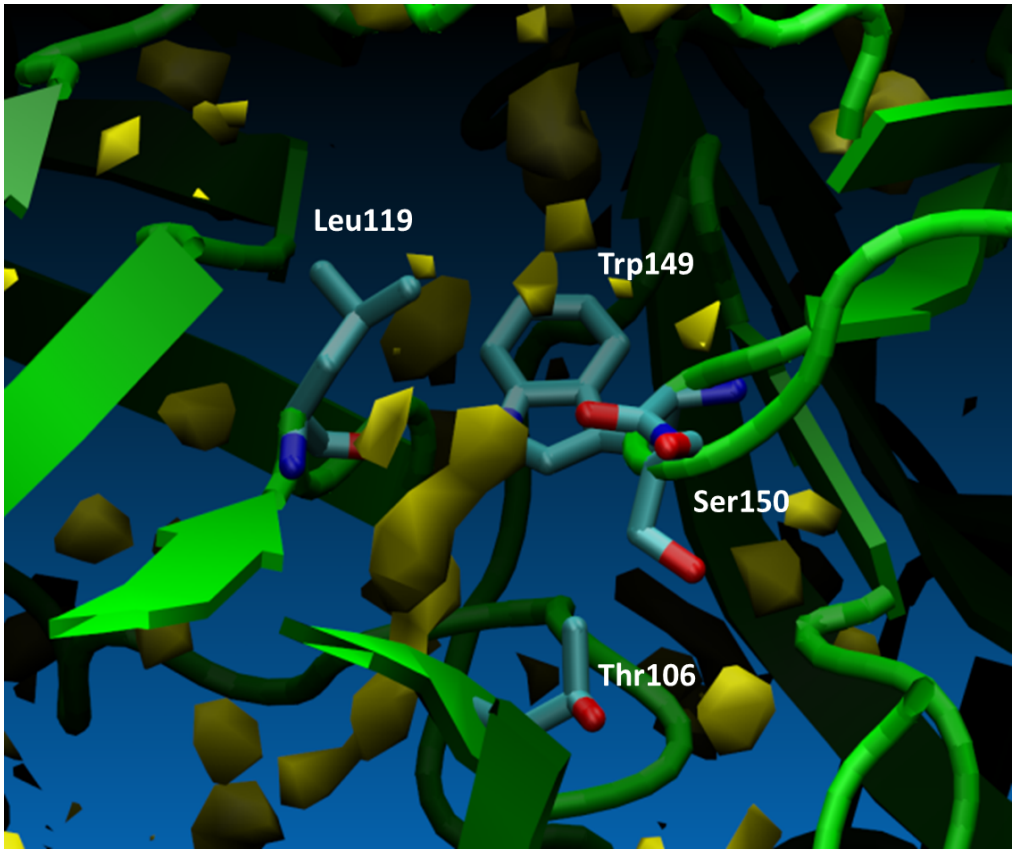

Figure 3
(Carlo Matera et al.)

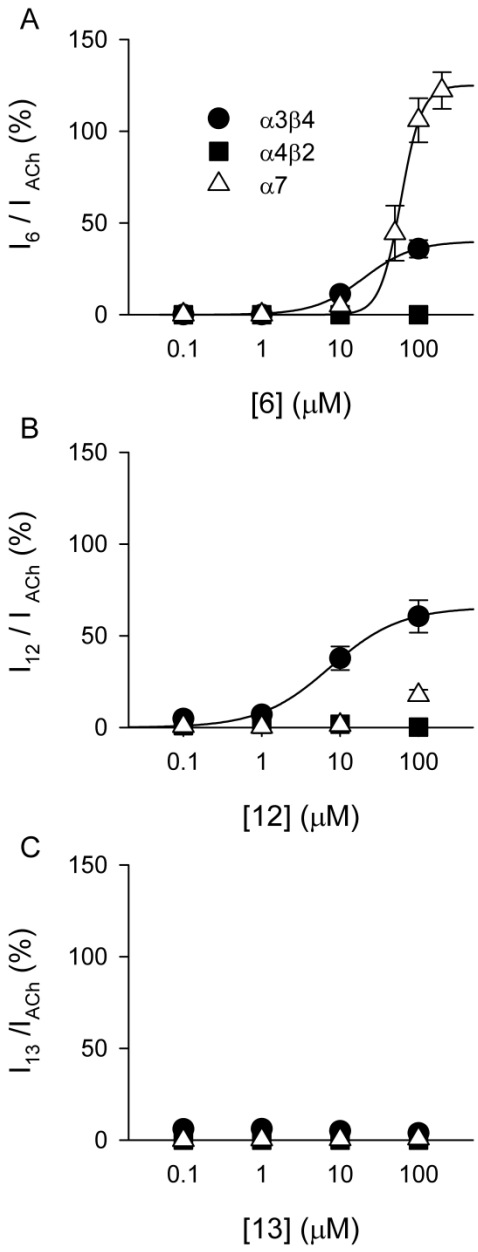

Figure 4
(Carlo Matera et al.)

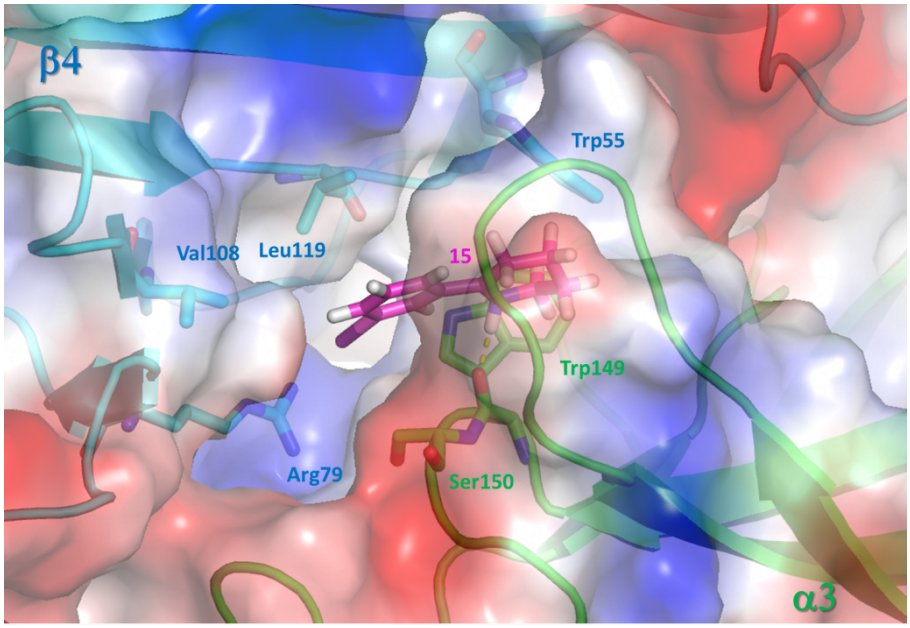

Figure 5
(Carlo Matera et al.)

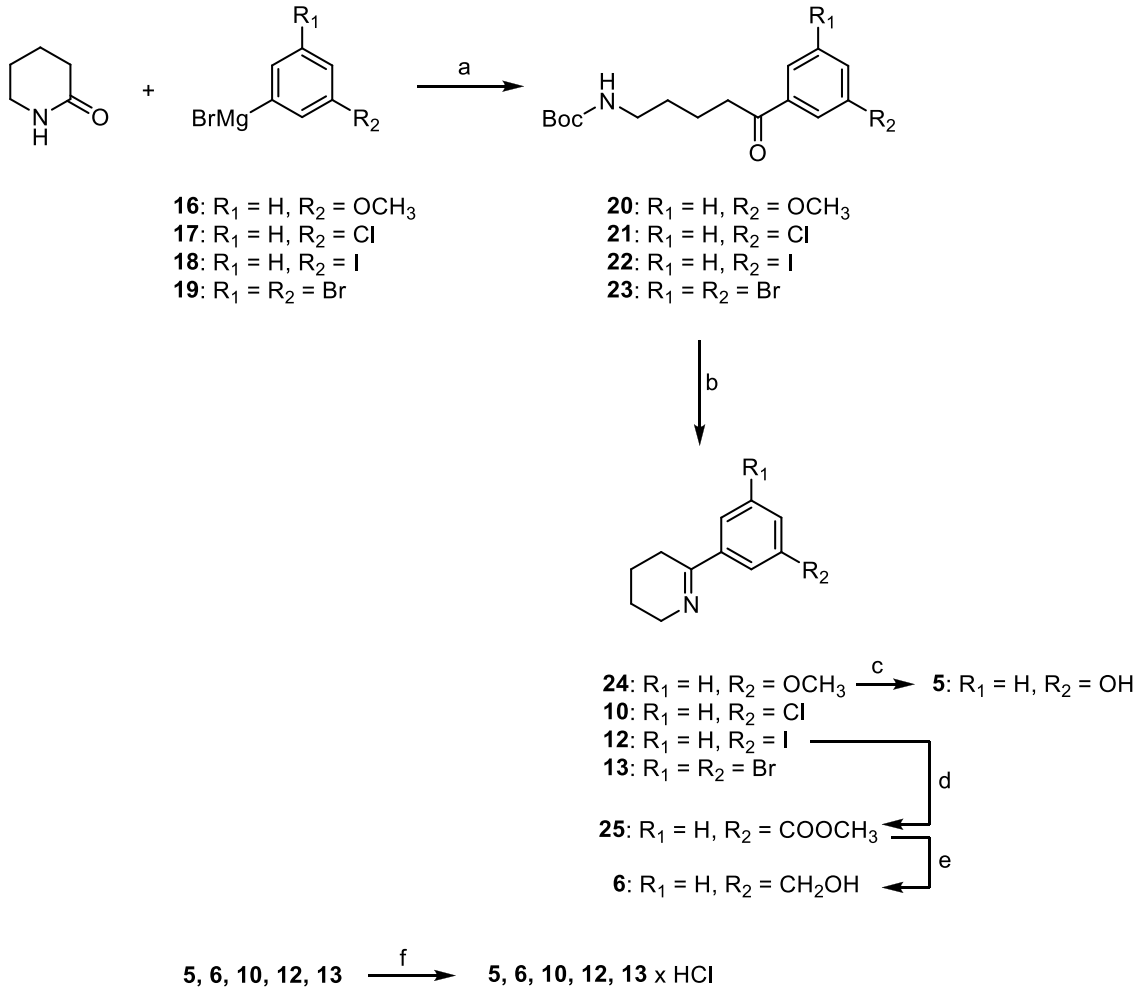

Scheme 1

(Carlo Matera et al.)

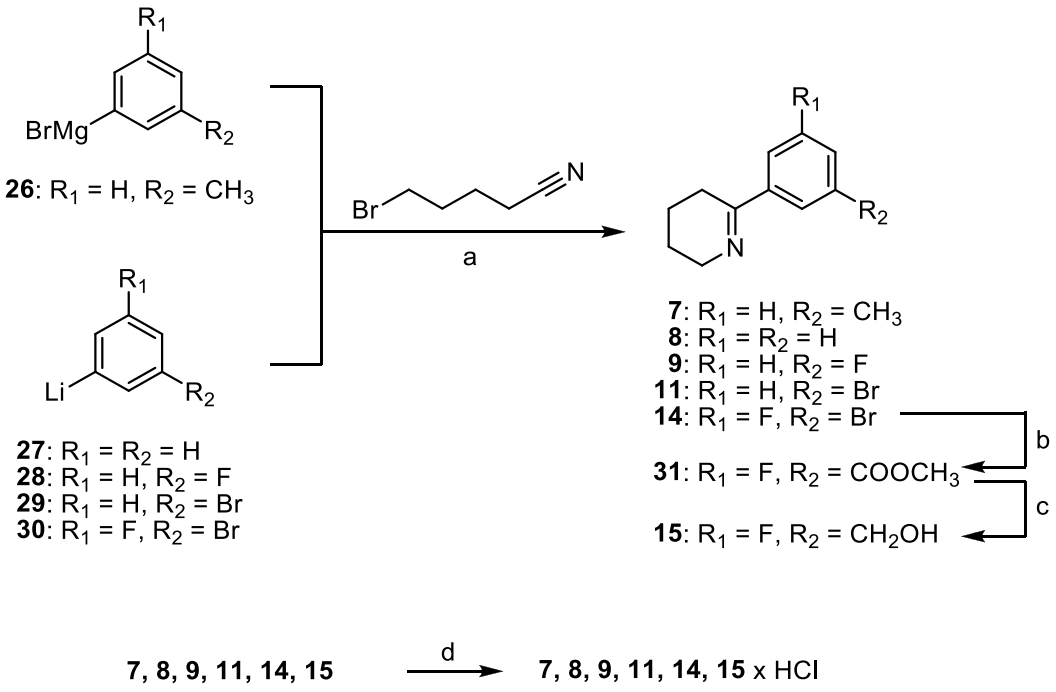

Scheme 2

(Carlo Matera et al.)